J. Fluid Mech. (1996), *vol.* 306, *pp.* 293–323

Numerical study of three-dimensional Kolmogorov flow at high Reynolds numbers

By VADIM BORUE AND STEVEN A. ORSZAG

Fluid Dynamics Research Center, Princeton University, Princeton, NJ 08544-0710, USA

(Received 11 March 1995 and in revised form 7 September 1995)

High-resolution numerical simulations (with up to 256^3 modes) are performed for three-dimensional flow driven by the large-scale constant force $f_y = F\cos(x)$ in a periodic box of size $L = 2\pi$ (Kolmogorov flow). High Reynolds number is attained by solving the Navier–Stokes equations with hyperviscosity $(-1)^{h+1}\Delta^h$ ($h = 8$). It is shown that the mean velocity profile of Kolmogorov flow is nearly independent of Reynolds number and has the 'laminar' form $v_y = V\cos(x)$ with a nearly constant eddy viscosity. Nevertheless, the flow is highly turbulent and intermittent even at large scales. The turbulent intensities, energy dissipation rate and various terms in the energy balance equation have the simple coordinate dependence $a + b\cos(2x)$ (with a, b constants). This makes Kolmogorov flow a good model to explore the applicability of turbulence transport approximations in open time-dependent flows. It turns out that the standard expression for effective (eddy) viscosity used in K–$\mathscr{E}$ transport models overpredicts the effective viscosity in regions of high shear rate and should be modified to account for the non-equilibrium character of the flow. Also at large scales the flow is anisotropic but for large Reynolds number the flow is isotropic at small scales. The important problem of local isotropy is systematically studied by measuring longitudinal and transverse components of the energy spectra and cross-correlation spectra of velocities and velocity–pressure-gradient spectra. Cross-spectra which should vanish in the case of isotropic turbulence decay only algebraically but somewhat faster than corresponding isotropic correlations. It is verified that the pressure plays a crucial role in making the flow locally isotropic. It is demonstrated that anisotropic large-scale flow may be considered locally isotropic at scales which are approximately ten times smaller than the scale of the flow.

1. Introduction

Naturally occurring open turbulent flows including jets and mixing layers are typically anisotropic and time dependent. Quite frequently they exhibit intermittent behaviour even at large scales. In this work we explore properties of open flows focusing on Kolmogorov flow, namely flow in a periodic box driven by a large-scale steady force $\propto \cos(x)$. By use of hyperviscous dissipation instead of Newtonian dissipation, the Reynolds number of the flow is effectively increased. At these high effective Reynolds numbers, Kolmogorov flow exhibits strong large-scale time dependence (intermittency). We find that for this flow, the effective (eddy) viscosity should be modified to account for the large-scale time dependence. We also address the question of verifying the local-isotropy hypothesis, which states that large-scale anisotropic flow becomes isotropic at small scales provided that the Reynolds number is sufficiently large.

More than 50 years ago, Kolmogorov (1941) proposed that three-dimensional homogeneous turbulence should have a universal, but singular, limit as viscosity tends to zero. In this zero-viscosity limit the total amount of energy dissipation has a finite non-zero limit. The mechanism of this 'dissipation without viscosity' is purely dynamical. It manifests itself through the energy flux from larger scales at which energy is input to smaller scales where it is dissipated. At intermediate spatial scales in the so-called inertial range, three-dimensional turbulence exhibits constant energy flux. The singularity of the zero-viscosity limit reveals itself in the fact that although viscosity is an irrelevant parameter in the inertial range, it eventually provides dissipation at the smallest scales of the system. In other words, viscosity provides the ultraviolet cutoff at a dissipation wavenumber k_d. In the inertial range, the fluid is effectively described by the inviscid equations while the direction of the energy flux imposes irreversibility on the flow. It is thus natural to suppose that the detailed way that energy is extracted from the system may not influence the properties of the inertial range.

In previous work (Borue & Orszag 1995*a*), we have already demonstrated that for given numerical resolution, we can effectively increase the extent of the inertial range of three-dimensional turbulence by an order of magnitude by using alternative forms of dissipation. With normal Newtonian viscosity it is necessary to have nearly two decades of wavenumbers in the dissipation range. This range of spatial modes is then not part of the inertial range. We propose replacing the normal Newtonian dissipation by a higher power of the Laplacian, i.e. a hyperviscosity. In this case, the dissipation range can be quite short and the remaining degrees of freedom can then participate in the inertial-range dynamics. Hyperviscosity is now a standard tool for numerical simulations of two-dimensional turbulence. The literature on the subject is extensive and too numerous to review here (see e.g. Borue 1993 and references therein). For three-dimensional turbulence, hyperviscosity was used by Herring & Metais (1989) for simulations of stratified turbulence (hyperviscosity was used concurrently with Newtonian viscosity to stabilize the calculations) and by Bartello, Metais & Lesieur (1994) for simulations of rotating turbulence. Also, the piecewise parabolic numerical scheme used for simulations of compressible turbulence by Porter, Pouquet & Woodward (1992) effectively involves fourth-order ($h = 2$) hyperviscosity.

It was shown by Borue & Orszag (1995*a*) that three-dimensional inertial-range dynamics is relatively independent of the form of the hyperviscosity and that modest resolution simulations with high-order hyperviscosity lead to sufficiently extensive inertial ranges that measurement of a broad variety of otherwise intractable quantities can be made. Similar conclusions may be drawn from the work by Bartello *et al.* (1994). On the other hand (Borue & Orszag 1995*a*) for the case of homogeneous isotropic white-in-time forced turbulence we observed deviations of the isotropic energy spectrum from the 5/3 Kolmogorov law (Kolmogorov 1941). It was suggested that this deviation is likely to be related to the large-scale behaviour of the system, in particular to the mechanism of energy pumping. Indeed, later (Borue & Orszag 1995*b*) we have shown that, for decaying turbulence in a periodic box, the 5/3 Kolmogorov law is recovered and self-similar decay is observed.

Here we concentrate on the case of large-scale anisotropic flow. In unpublished work from the 1950s, Kolmogorov proposed to study flow in a periodic box with large-scale forcing $f_y = \cos(k_f x)$ as a model to understand the transition to turbulence. This flow is now referred to as Kolmogorov flow (Meshalkin & Sinai 1961). It was shown by Meshalkin & Sinai (1961) that this flow is unstable to large-spatial-scale

perturbations. Most of the literature on Kolmogorov flow concentrates on the case of two-dimensional flow (see e.g. E & Shu 1993 and references therein). In three-dimensions, Kolmogorov flow was studied only for a small-scale force in connection with the possibility of anisotropic inverse cascade and large-scale symmetry breaking (Sulem *et al.* 1989). Here we consider high Reynolds number three-dimensional Kolmogorov flow generated by the force $f_y = \cos(x)$ in a periodic box of size $L = 2\pi$. The force acts on the largest possible scale of the system. In two dimensions this flow is unconditionally stable, but it does become turbulent in three dimensions. The use of hyperviscosity enables very high Reynolds number simulations. When highly turbulent, the mean flow and turbulent intensities of Kolmogorov flow have an unusually simple structure. As an open flow, Kolmogorov flow is then an interesting testing ground for turbulence transport models and large-eddy simulations. However, such tests are left for the future. In this paper we concentrate on the study of various mean flow characteristics, including the turbulent energy budget. Also we address the question of local isotropy of large-scale anisotropic flow.

The local isotropy hypothesis states that, at sufficiently high Reynolds numbers, small-scale structures of turbulent motions are independent of large-scale anisotropy (see Kolmogorov 1941, 1962 and also Monin & Yaglom 1975). This hypothesis plays a key role in nearly all theories, models, and large-eddy simulations of turbulence. If this hypothesis breaks down there is very little hope of obtaining a universal theory of turbulence since the small-scale flow will then always be dependent on the details of the anisotropic large-scale structures. Since Kolmogorov proposed his theory, there have been many experiments conducted in different systems to verify the local-isotropy hypothesis. Excellent reviews of this work already exist (see Van Atta 1991 and Sreenivasan 1991 and references therein). However, up to now there has been no consensus on whether the local-isotropy hypothesis is valid. An important contribution to this problem was recently made by Saddoughi & Veeravalli (1994). These authors not only demonstrated how local isotropy is established in anisotropic shear flow when the Reynolds number increases, but they also found scaling laws for the decay of anisotropic contributions.

There have also been a number of recent theoretical and numerical studies that address the problems of the relative importance of non-local versus local (in wavenumber space) interactions in the energy cascade process. In some studies, non-local interactions in the energy cascade process have been inferred, thereby calling into question local self-similar energy cascades and the local-isotropy hypothesis (see Brasseur & Wei 1994 for a review). Unfortunately, the Reynolds numbers in these numerical simulations using Newtonian viscosity are too low to reliably verify or reject the local-isotropy hypothesis.

In this paper we systematically study local isotropy as a function of the Reynolds number. It is demonstrated that Kolmogorov flow which is highly anisotropic at large scales becomes locally isotropic at small scales. As found by Saddoughi & Veeravalli (1994) we also find that anisotropic correlations decay in wavenumber space only algebraically and only slightly faster than isotropic correlations. This suggests that although the local-isotropy hypothesis seems to hold, the slow decay of anisotropic fluctuations may have an impact even inside the inertial range. The importance of large-scale shear and the algebraic character of the decay of anisotropic corrections were extensively discussed by Yakhot (1994) and Grossman *et al.* (1994).

2. Technical background

The hyperviscosity-modified Navier–Stokes equations are

$$\partial_t v_i + v_j \partial_j v_i = -\partial_i p + (-1)^{h+1} \nu_h \Delta^h v_i + f_i \tag{2.1}$$

where the pressure p is calculated from the incompressibility condition $\partial_i v_i = 0$. Summation over repeated indices is assumed. On the right-hand side of (2.1) we include a force which is non-zero only at some characteristic scale k_f and a hyperviscous dissipation designed to provide an energy sink at small scales. For the case of Kolmogorov flow, the only non-zero component of the force is $f_y = F\cos(k_f x)$ with $k_f = 1$. The power h of the hyperviscous dissipation is chosen to maximize the extent of the inertial range. In general larger h yields a larger inertial range, but there are practical considerations that limit h. We solve (2.1) using a parallel pseudospectral code described by Jackson, She & Orszag (1991). To justify the use of the spectral numerical scheme, exponential decay of spectra must start no latter than wavenumber $N/3$, the dealiasing threshold for spatial resolution N^3. These requirements lead us to chose the power of hyperviscosity $h = 8$, which is assumed throughout the paper. For $h = 8$, the hyperviscous dissipation is nearly zero at wavenumbers $k \leqslant N/3$ and abruptly turns on at $k \geqslant k_d \approx N/3$. The hyperviscosity coefficient ν_h with $h = 8$ is chosen so that $\nu_h (N/2)^{2h} \delta t \approx 0.5$, where δt is the time step of the numerical scheme. The time step on the other hand is fixed by the characteristic maximum velocity at large scales v_{max} according to the Courant number criterion: $v_{max}\delta t N/2\pi \leqslant 0.2$. Thus all parameters of equation (2.1) are uniquely defined by the large-scale flow and the numerical resolution.

In a statistically steady state, there must be a constant energy flux

$$J_E(k) = \int_{k'>k}^{\infty} T(k')\mathrm{d}k' \tag{2.2}$$

for $k_f < k < k_d$. Here $T(k)$ is the energy transfer function. On the basis of Kolmogorov's (1941) scaling theory for the inertial range, we expect that the isotropic energy spectrum $E(k)$ has the form

$$E(k) = 4\pi k^2 \langle v_i(-\boldsymbol{k}) v_i(\boldsymbol{k}) \rangle = \frac{\bar{\mathscr{E}}^{2/3}}{k^{5/3}} G(k/k_d, k_d/k_f) \tag{2.3}$$

with possible anomalous dimensions (deviations of the scaling laws from Kolmogorov scaling) included in the function G. Here $\bar{\mathscr{E}}$ is the mean energy dissipation rate set by the external forcing. In the case of anisotropy we expect anisotropic spectra at least at low wavenumbers. In the Kolmogorov (1941) theory at low wavenumbers G approaches a universal constant C_K now called the Kolmogorov constant. We define the energy dissipation rate in the case of hyperviscosity as

$$\mathscr{E} = \nu_h \Delta^{h/2} v_i \Delta^{h/2} v_i. \tag{2.4}$$

For Newtonian viscosity the energy dissipation rate is defined as

$$\mathscr{E}_n = 2\nu S_{ij} S_{ij}. \tag{2.5}$$

The rate of strain S_{ij} and vorticity ω_i are defined as

$$S_{ij} = \frac{1}{2}\left(\frac{\partial v_i}{\partial x_j} + \frac{\partial v_j}{\partial x_i}\right); \quad \omega_i = \varepsilon_{ijk}\partial_j v_k. \tag{2.6}$$

It is interesting to determine the Reynolds number when hyperviscosity is used. The Taylor microscale Reynolds number for Newtonian viscosity is defined as

$$R_\lambda = \frac{v_{rms}\lambda}{\nu} \tag{2.7}$$

based on the Taylor microscale

$$\lambda = \left(\frac{15v_{rms}^2}{\omega_{rms}^2}\right). \tag{2.8}$$

Here v_{rms} and ω_{rms} are root-mean-square velocity and vorticity. It is convenient to rewrite (2.7) and (2.8) using the dissipation cutoff k_d. We define the dissipation cutoff k_d as the wavenumber at which the maximum of the vorticity spectrum $k^2E(k)$ is attained. In the case of Newtonian viscosity $k_d \sim (\bar{\mathscr{E}}/\nu^3)^{1/4}$. Estimating $v_{rms} \sim \bar{\mathscr{E}}^{1/3}/k_f^{1/3}$ and $\omega_{rms} \sim \bar{\mathscr{E}}^{1/3}k_d^{2/3}$, from (2.8) and (2.7) we obtain $\lambda \sim 1/(k_f^{1/3}k_d^{2/3})$ and $R_\lambda \sim (k_d/k_f)^{2/3}$. We suggest that the Taylor microscale Reynolds number for hyperviscosity be defined as

$$R_\lambda = C_h\left(\frac{k_d}{k_f}\right)^{2/3}, \tag{2.9}$$

where C_h may be different for different powers of hyperviscosity. We also suggest fixing C_h by comparing the ranges of constant energy flux, which scale nearly linearly with k_d. As was shown by Borue & Orszag (1995*a*), $C_1 \approx 25$ and $C_8 \approx 50$. These are rather crude estimates. Nevertheless the definition (2.9) is convenient for comparing different runs with the same power of hyperviscosity. We expect that our largest 256^3 resolution run with $h = 8$ should approximately correspond to $R_\lambda \approx 1000$, $k_d \approx 80$ (here and later we assume that wavenumbers are measured in $2\pi/L = 1$ units).

Kolmogorov flow is inhomogeneous and anisotropic, with translational invariance broken in the x-direction. Translational invariance is still valid in the y- and z-directions. Even without translational invariance in the x-direction we may still use spectra measured in this direction, but we should remember that these spectra have the form $P(x)S(k_x)$. Here $P(x)$ is a slowly varying prefactor reflecting the loss of translational symmetry and $S(k_x)$ is the spectrum itself. This decomposition is accurate only if prefactors vary slowly in comparison with $S(k_x)$. In our case, prefactors have the characteristic scale of forcing k_f. Thus the decomposition becomes sufficiently accurate for $k_x > k_f$. In what follows we will assume such a decomposition for spectra in the x-direction. Assuming that our system is approximately homogeneous in the x-direction we may introduce nine one-dimensional energy spectra. The energy spectrum of the i-component of velocity measured in the α-direction takes the form

$$E_{ii}^{\alpha}(k_\alpha) = \int \langle v_i(-\boldsymbol{k})v_i(\boldsymbol{k})\rangle \prod_{\ell\neq\alpha} \mathrm{d}k_\ell. \tag{2.10}$$

There is no summation over i and α in (2.10). Throughout the paper we use the notation $i = x, y, z$ (lower index) for the i-component of velocity and $\alpha = X, Y, Z$ (upper index) for the direction in which the one-dimensional energy spectrum is measured. When $i = \alpha$ these spectra are called longitudinal spectra $E_{LL}(k)$, otherwise for $i \neq \alpha$ they are called transverse spectra $E_{NN}(k)$ (Monin & Yaglom 1975). For isotropic flow, all longitudinal spectra should coincide. The same is true for all the

transverse spectra. For solenoidal vectors, it is possible to calculate the transverse spectrum from the longitudinal one (Monin & Yaglom 1975) as

$$E_{NN}(k) = \tfrac{1}{2}E_{LL}(k)\left(1 - \frac{\mathrm{d}\log E_{LL}(k)}{\mathrm{d}\log k}\right). \tag{2.11}$$

Also, the isotropic energy spectrum may be calculated from the longitudinal and transverse energy spectra according to

$$E(k) = -\frac{1}{2}\frac{\mathrm{d}(E_{LL}(k) + 2E_{NN}(k))}{\mathrm{d}\log k} \tag{2.12}$$

We will use (2.11) and (2.12) to check the local isotropy of our system.

It is also convenient to define the one-dimensional spectrum of any two operators A and B measured in the direction α ($\alpha = X, Y, Z$) as

$$\mathscr{C}^{\alpha}[A,B](k_{\alpha}) = \int \tfrac{1}{2}\langle A(-\mathbf{k})B(\mathbf{k}) + A(\mathbf{k})B(-\mathbf{k})\rangle \prod_{\ell\neq\alpha} \mathrm{d}k_{\ell}. \tag{2.13}$$

The only non-zero Reynolds stress for the Kolmogorov flow is $\langle v_x v_y\rangle$. To characterize anisotropy we also introduce the correlation-coefficient spectrum between the x- and y-velocity components which can be measured in the Y- or Z-directions. For the direction $\alpha = Y, Z$ it has the form

$$R^{\alpha}_{xy}(k_{\alpha}) = \frac{\mathscr{C}^{\alpha}[v_x, v_y](k_{\alpha})}{[E^{\alpha}_{xx}(k_{\alpha})E^{\alpha}_{yy}(k_{\alpha})]^{1/2}}. \tag{2.14}$$

For local isotropy to hold this spectrum should fall to zero at high wavenumbers.

3. Kolmogorov flow

The Kolmogorov flow is characterized by the amplitude of the force, the scale of the force and the Reynolds number. The force has the form

$$f_y = F\cos(k_f x); \qquad k_f = 1; \qquad F = 0.16. \tag{3.1}$$

The amplitude of the force F defines the time scale of the problem and may be chosen arbitrarily. The Reynolds number is defined by the available numerical resolution. The characteristic velocity and time scale in the case of Kolmogorov flow are

$$V_0 = 2.5\frac{F^{1/2}}{k_f^{1/2}}; \qquad \tau_0 = \frac{1}{k_f V_0} = \frac{1}{(Fk_f)^{1/2}} \tag{3.2}$$

We choose the prefactors in (3.2) arbitrarily. In our numerical simulations we used $F = 0.16$ and $k_f = 1$, which correspond to $V_0 = 1$ and $\tau_0 = 1$. To obtain results that are independent of the amplitude of the force we need to rescale all relevant quantities appropriately. In fact we assume that we are using the units (3.2) so that all our results are automatically rescaled.

We report here a series of runs for Kolmogorov flow with different numerical resolutions (Reynolds numbers) using hyperviscous dissipation and a few runs with Newtonian dissipation. Our numerical resolutions are 64^3, 128^3 and 256^3. The characteristic velocity for $F = 0.16$ is $v_{rms} \approx 0.5$ and the characteristic large-eddy turnover time $\tau_e \approx 1/v_{rms} \approx 2$. We integrate for more than 1000 large-eddy turnover times for 64^3 resolution, 500 large-eddy turnover times for resolution 128^3 and around 10 large-eddy turnover times for resolution 256^3. Low Reynolds number simulations

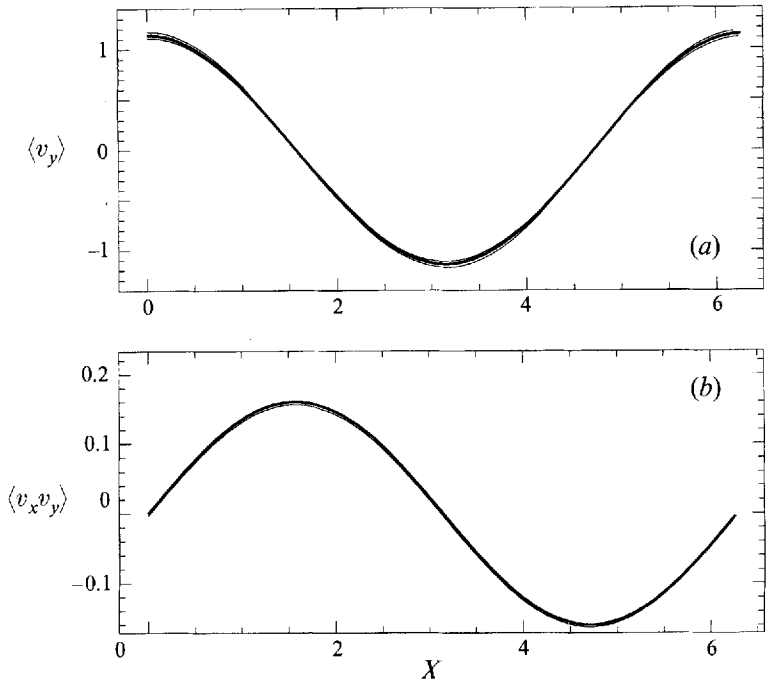

FIGURE 1. (*a*) Mean velocity profiles; (*b*) average Reynolds stresses. The data are plotted for the hyperviscosity ($h = 8$) runs with resolutions 128^3 and 64^3. The thick lines correspond to the interpolation formulas (3.5) and (3.6).

with 64^3 and 128^3 resolution with Newtonian viscosity has also been performed for up to 500 large-eddy turnover times. Mostly we will consider the $h = 8$ hyperviscous simulations with 64^3 and 128^3 resolution, because the averaging time in these cases is long enough to obtain statistically convergent results even for sensitive quantities. For the 256^3 case the time of integration is sufficient to obtain spectral characteristics of the flow, but it is still too small to obtain reliable turbulence intensities. When $h = 8$, the dissipation scale k_d, defined as the maximum of the enstrophy spectrum, is $k_d = 21, 41, 82$ for $64^3, 128^3, 256^3$ resolution, respectively.

3.1. *Mean velocity and turbulence intensities*

In laminar Kolmogorov flow (with Newtonian viscosity) the velocity has the form

$$v_y = \frac{F}{\nu k_f^2} \cos(k_f x). \tag{3.3}$$

At high Reynolds number the flow becomes turbulent and a fluctuating Reynolds stress ($\langle v_x v_y \rangle$) is generated; here $\langle ... \rangle$ indicates an appropriate average, which in the case of Kolmogorov flow is a combined space–time average over t, y, z. In the usual way an effective or eddy viscosity is introduced through the relation

$$\langle v_x v_y \rangle = -\nu_{eff} \frac{\mathrm{d} \langle v_y \rangle}{\mathrm{d}x}. \tag{3.4}$$

The numerical results for the mean velocity and Reynolds stress plotted in figure 1 show that for high Reynolds number Kolmogorov flow the mean velocity has the

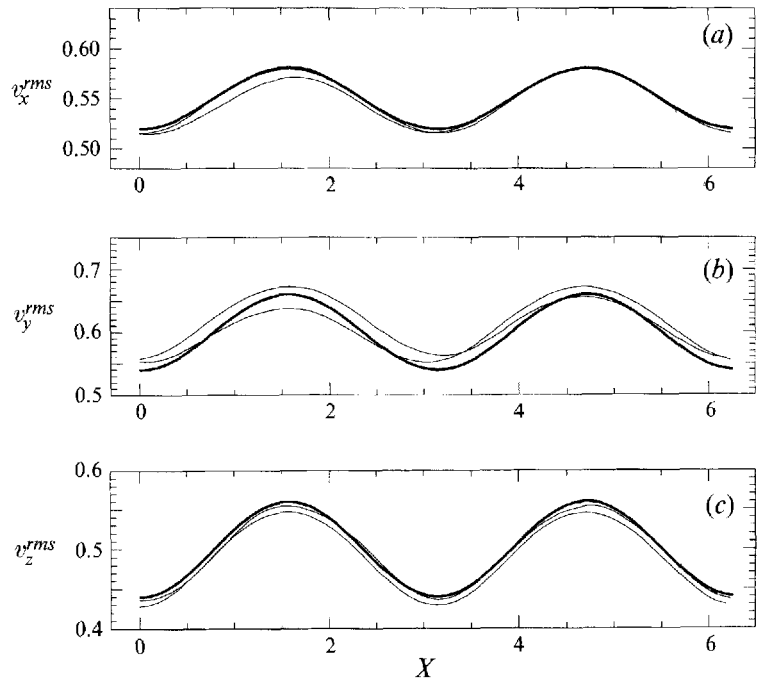

FIGURE 2. Turbulence intensities: (*a*) v_x^{rms}; (*b*) v_y^{rms}; (*c*) v_z^{rms}. The data are plotted for the hyperviscosity ($h = 8$) runs with resolutions 128^3 and 64^3. The thick lines correspond to the interpolation formulas (3.9).

nearly laminar profile ($k_f = 1$ is assumed)

$$\langle v_y \rangle = (1.1 \pm 0.05) V_0 \cos(x) \tag{3.5}$$

and the Reynolds stress is given approximately by

$$\langle v_x v_y \rangle = 0.16 V_0^2 \sin(x). \tag{3.6}$$

Here V_0 is given by (3.2) and the result (3.6) follows from the space–time averaged Navier–Stokes equation

$$\frac{\mathrm{d}\langle v_x v_y \rangle}{\mathrm{d}x} = F \cos(x). \tag{3.7}$$

We conclude from (3.4)–(3.6) that the effective viscosity is nearly constant:

$$\nu_{eff} = (0.14 \pm 0.01) V_0^2 \tau_0. \tag{3.8}$$

We emphasize that long averaging times are required to obtain statistically reliable mean velocity and Reynolds stress results.

In figure 2 we plot the (x, y, z)-components of the turbulent r.m.s. velocity fluctuations. These r.m.s. velocities are well approximated by

$$\left.\begin{aligned} v_x^{rms} &= 0.55(1 - 0.055\cos(2x))V_0, \\ v_y^{rms} &= 0.6(1 - 0.1\cos(2x))V_0, \\ v_z^{rms} &= 0.5(1 - 0.1\cos(2x))V_0. \end{aligned}\right\} \tag{3.9}$$

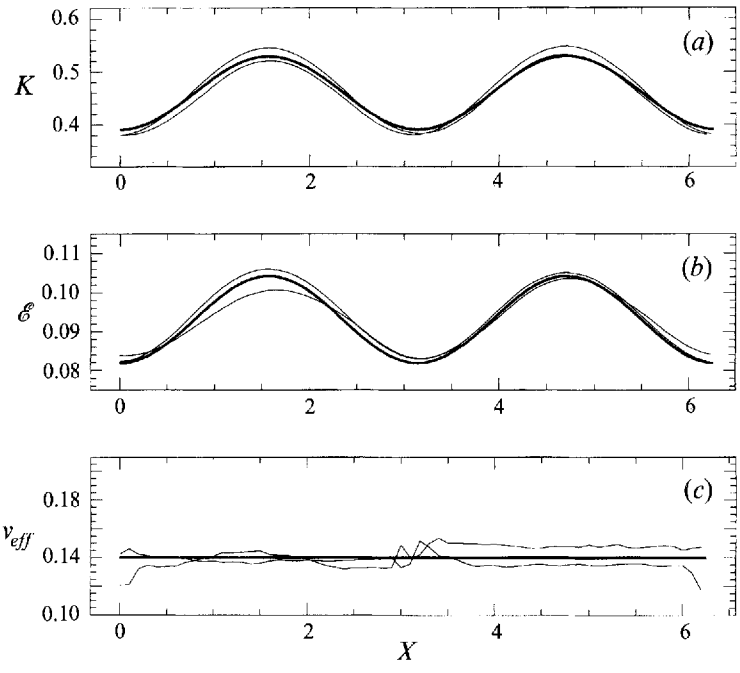

FIGURE 3. Averaged (*a*) total turbulent kinetic energy; (*b*) energy dissipation rate; (*c*) effective viscosities. The thick lines correspond to the interpolation formulas (3.10), (3.11) and (3.8). The data are plotted for the hyperviscosity ($h = 8$) runs with resolutions 128^3 and 64^3.

The total turbulent energy, plotted in figure 3(*a*), is well approximated by

$$K = 0.46(1 - 0.15\cos(2x))V_0^2 \tag{3.10}$$

while the averaged energy dissipation rate $\mathscr{E}$, defined by (2.4) and plotted in figure 3(*b*) has the form

$$\mathscr{E} = 0.093(1 - 0.12\cos(2x))V_0^3 k_f. \tag{3.11}$$

The scatter observed in figure 3(*a*, *b*) is likely due to strong fluctuations at large scales that are not sufficiently averaged in the limited time of our simulations.

The effective viscosity calculated by (3.4) is plotted in figure 3(*c*) for the hyperviscous runs with resolution 128^3 and 64^3. It is clear that the effective viscosity is nearly constant and given by (3.8).

Kolmogorov flow is well suited as a test-bed for various approximate models that are used for empirical description of turbulent flows. One of the basic assumptions of these transport models is that the turbulent eddy viscosity is given by (see for example Yakhot *et al.* 1992)

$$\nu_{eff} = C_\mu \frac{K^2}{\mathscr{E}}. \tag{3.12}$$

In the RNG turbulence theory, $C_\mu \approx 0.085$ (Yakhot & Orszag 1986). However it must be emphasized that the formula (3.12) is only justifiable for equilibrium turbulence in which the characteristic space and time scales over which mean quantities vary are large compared to the scales of energetic turbulent eddies. In non-equilibrium flows deviations are expected.

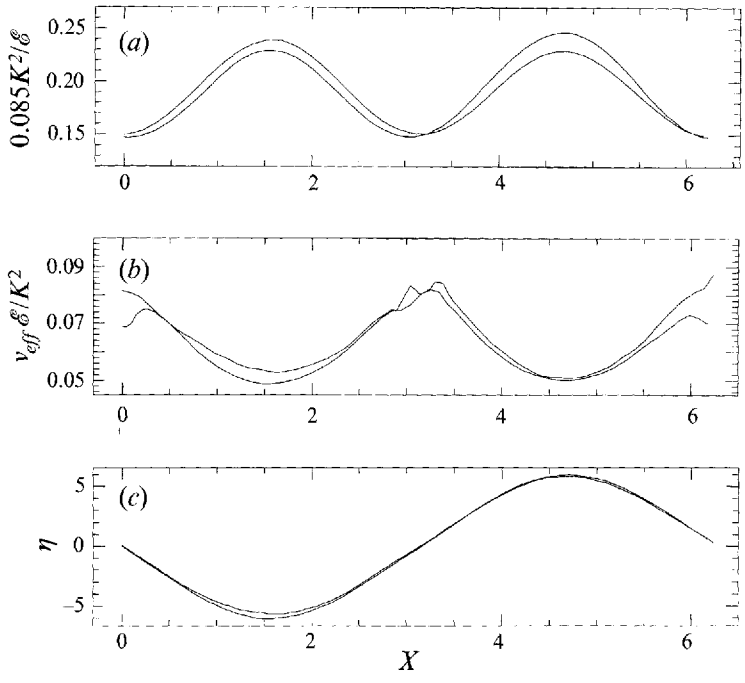

FIGURE 4. (*a*) $0.085K^2/\mathscr{E}$, (*b*) $C_\mu = \nu_{eff}\mathscr{E}/K^2$, (*c*) η as functions of x. The data are plotted for the hyperviscosity ($h = 8$) runs with resolutions 128^3 and 64^3.

As was suggested by Smith & Yakhot (1993), using an extension of RNG theory, the effective viscosity for non-equilibrium flows has the same form (3.12) but C_μ depends on the dimensionless shear

$$\eta = \left\langle \frac{\partial v_y}{\partial x} \right\rangle \frac{K}{\mathscr{E}} \tag{3.13}$$

according to

$$C_\mu(\eta) = 0.085\left[1 - \exp(-\frac{c_\eta}{|\eta|})\right]. \tag{3.14}$$

Here c_η is some constant of order one.

In figure 4(*a*) we plot the effective viscosity calculated *a posteriori* by equation (3.12). We see that (3.12) leads to a space-varying effective viscosity inconsistent with the experimentally observed constant effective viscosity (3.8). Using equations (3.8) and (3.12) $C_\mu = \nu_{eff}\mathscr{E}/K^2$ depends on x. The functions $C_\mu(x)$ and $\eta(x)$ are plotted in figures 4(*b*) and 4(*c*), respectively. For our Kolmogorov flow C_μ varies from 0.085, for $\eta = 0$, down to 0.05, when η is maximal.

In figure 5(*a*) we plot the measured C_μ coefficient as a function of η. Although we performed quite long statistical averaging some asymmetry of the curve still may be observed, indicating that these data are sensitive to the total averaging time. The results plotted in figure 5(*a*) may be fitted by the simple linear approximation

$$C_\mu \approx 0.085(1 - 0.065|\eta|). \tag{3.15}$$

For comparison, $C_\mu(\eta)$ as predicted by (3.14) with $c_\eta = 5$ is plotted in figure 5(*b*). In the range of η observed in Kolmogorov flow ($|\eta|_{max} \approx 5.5$) (3.14) is not inconsistent with our data. The largest errors come from the low-shear regions where our

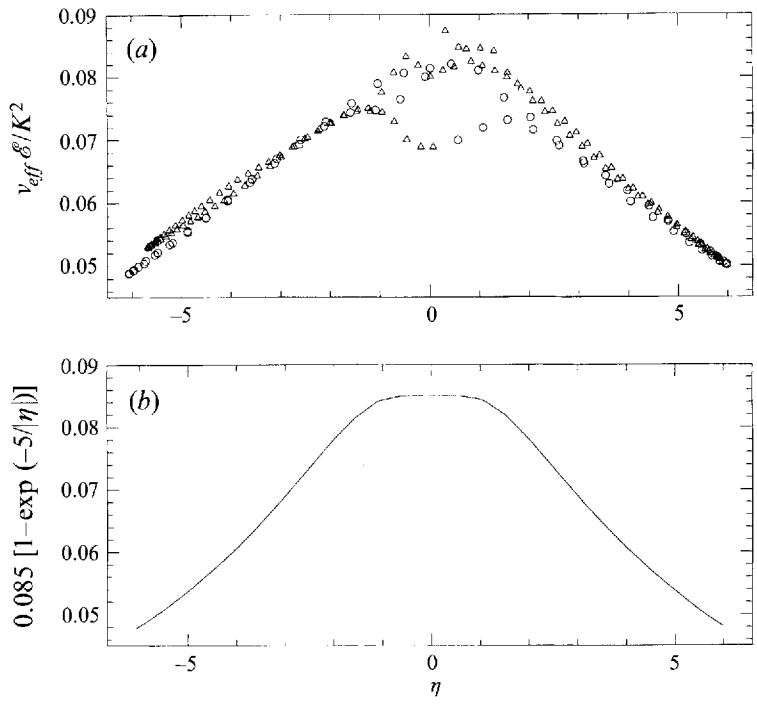

FIGURE 5. (*a*) $C_\mu = \nu_{eff}\mathscr{E}/K^2$ as a function of η; (*b*)RNG theoretical prediction (3.14). The data are plotted for the hyperviscosity ($h = 8$) runs with resolutions 128^3 and 64^3.

data have the largest experimental uncertainty. Similar decrease of C_μ with $|\eta|$ was observed in numerical simulations by Cazalbou & Bradshaw (1993) in the wall region of channel flow where η is high and in experiments on different types of shear flow by K. Sreenivasan (1995, personal communication).

3.2. *Large-scale intermittency of Kolmogorov flow*

In Kolmogorov flow velocity fluctuations are nearly of the same order of magnitude as the mean velocity itself. This high level of turbulence is rarely observed in wall-bounded flows, but is common in open flows. Kolmogorov flow demonstrates highly intermittent behaviour in time even at large scales. In our simulations we recorded the total energy and enstrophy of the flow as a function of time. We also recorded the mean energy as a function of time. The mean energy of the flow at a given moment of time is defined as the energy of the mode $k_x = 1$ averaged over the y- and z-directions. The turbulent energy of the flow is defined as the difference between the total energy and the mean energy of the flow. In this section we analyse these signals for a hyperviscous run with resolution 64^3. For runs with other resolutions these quantities behave similarly. The total, mean and turbulent energies and total enstrophy for this run are plotted in figure 6(*a–d*).

For these signals probability distribution functions are not very far from Gaussian although substantial skewness $\gamma_1 = \mu_3/\sigma^3$ and excess flatness $\gamma_2 = \mu_4/\sigma^4 - 3$ can be observed. Here μ_n is the nth order central moment and σ is the variance. The largest skewness and excess flatness are for the turbulent energy signal: $\gamma_1 \approx 0.8$ and $\gamma_2 \approx 1.2$. For the mean energy signal, deviations from Gaussian statistics are smaller: $\gamma_1 \approx 0.6$ and $\gamma_2 \approx 0.2$. For the total energy signal,

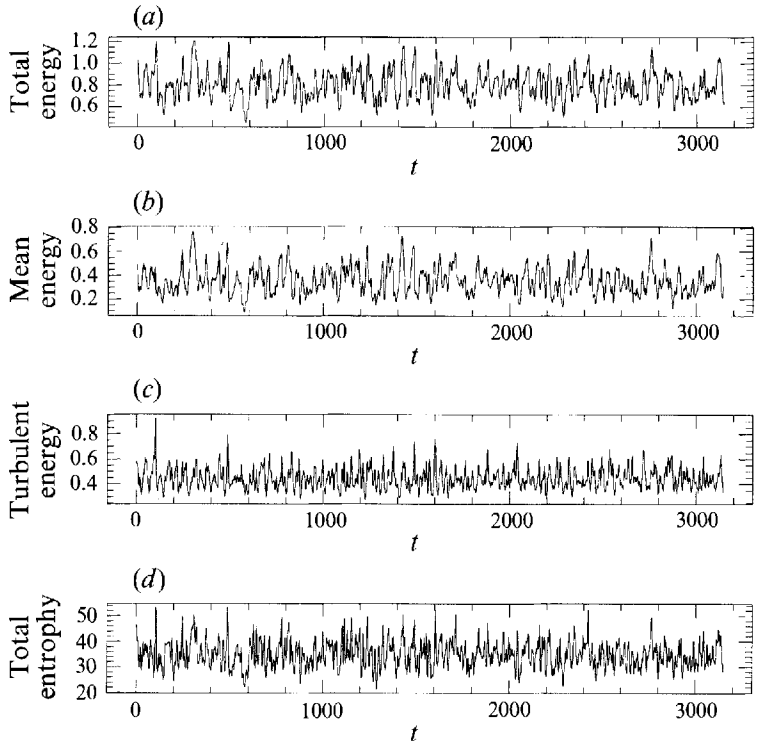

FIGURE 6. (*a*) Total energy, (*b*) mean energy, (*c*) turbulent energy, (*d*) total enstrophy as a function of time. Time is measured in units of τ_0.

$\gamma_1 \approx 0.25$ and $\gamma_2 \approx -0.14$, substantially smaller than for each of the components. Thus the mean and turbulent energy signals should be strongly correlated. The statistics of the total enstrophy signal is also close to Gaussian: $\gamma_1 \approx 0.34$ and $\gamma_2 \approx 0.1$.

To characterize cross-correlations of these signals we calculate their power spectral densities and cross-spectral densities. The power spectral density of a signal $\xi(t)$ is defined as $P(\xi|\omega) = \langle|\xi^*(\omega)\xi(\omega)|\rangle$ and the cross-spectrum density of this signal with another signal $\zeta(t)$ is defined as $C(\xi,\zeta|\omega) = \langle\zeta(\omega)\xi^*(\omega)\rangle$ (with ensemble averages assumed). The coherence function of these signals is defined as $|C(\xi,\zeta|\omega)|^2/(P(\xi|\omega)P(\zeta|\omega))$. The phase correlations between variables are characterized by the phase ϕ of the cross-spectrum $C(\xi,\zeta|\omega)$. We use standard Gaussian windows to perform Fourier transforms.

In figure 7(*a*, *b*) we plot the coherence function and the phase correlation function of the mean energy and turbulent energy signals. At high frequencies, there is strong coherence between these quantities with a phase correlation ϕ of approximately $-\pi$. Thus, at high frequencies, whenever the mean energy is large, the turbulent energy is small and vice versa. The coherence and phase correlation functions of the total energy and the total enstrophy signals are plotted in figure 7(*c*, *d*). These two signals are also strongly coherent with a characteristic phase shift of approximately $-\pi/2$. The total enstrophy signal is strongly correlated with the time derivative of the total energy signal (as is expected from the proportionality of energy dissipation rate and the total enstrophy, even for hyperviscosity).

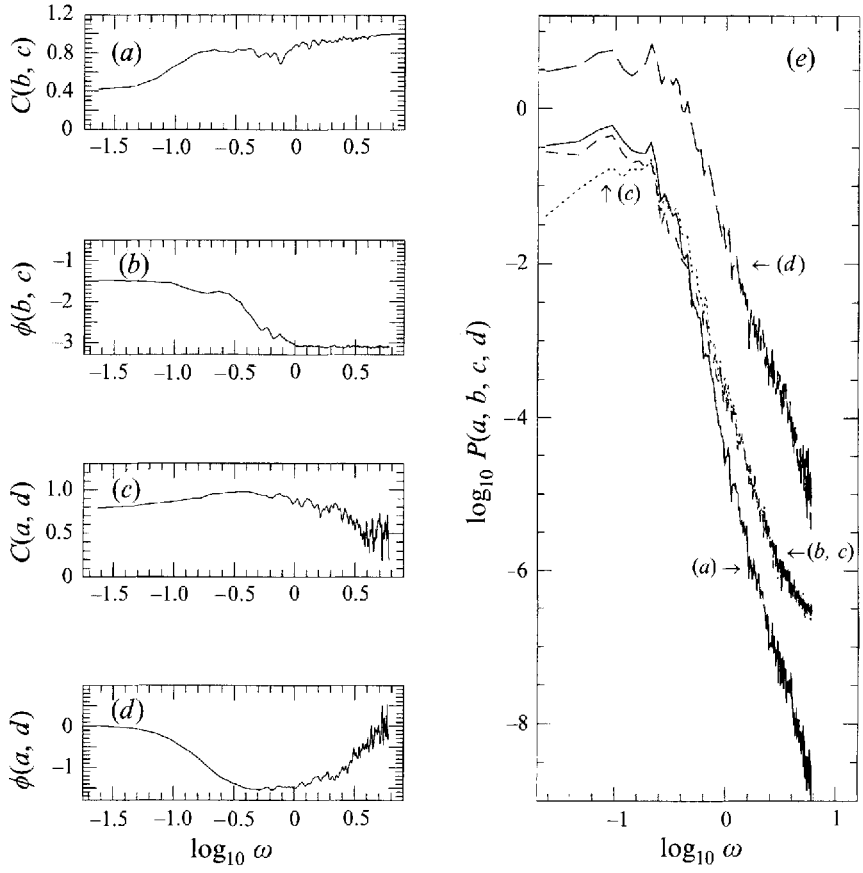

FIGURE 7. (*a*) Coherence function between the mean energy and turbulence energy signals. (*b*) Phase correlation function between the mean energy and turbulence energy signals. (*c*) Coherence function between the total energy and total enstrophy signals. (*d*) Phase correlation function between the total energy and total enstrophy signals. (*e*) Power spectra of signals in figure 6 as functions of frequency on a $\log_{10} - \log_{10}$ scale. Power spectra are labelled in accordance with the labels (*a–d*) in figure 6.

Power spectra of the signals in figure 6 are plotted in figure 7(*e*). We may see that the power spectra of the mean and turbulent energies nearly coincide and scale approximately as $1/\omega^2$. The power spectrum of the total enstrophy also scales roughly as $1/\omega^2$. In contrast, the power spectrum of the total energy is substantially steeper $\sim 1/\omega^3$. The $1/\omega^2$ behaviour of power spectra reflects sharp (like θ-function) jumps in signals. During these jumps the energy may change by a factor of 2–3 over a large-eddy turnover time. The extent of the low-wavenumber flat part of the spectra characterizes the autocorrelation time of the system, which is approximately 30. Thus after roughly 15 large-eddy turnover times the flow reaches a new statistically independent state.

A simple qualitative picture of Kolmogorov flow emerges from this correlation analysis. At some times, Kolmogorov flow has a relatively low level of turbulence with strong, increasing mean flow. At this stage the energy provided by the force accumulates in the mean flow. Then, at a certain level of the mean shear, the flow abruptly becomes unstable producing high-intensity turbulence. During these

'bursting' events a significant portion of the mean flow energy is transferred to the turbulent energy on the time scale of several large-eddy turnover times. After such a 'burst' the turbulent energy decays due to viscosity and the mean energy of the flow starts increasing again. The 'bursting' events are stochastic and intermittent in time. It is natural that this 'bursting' phenomenon is called large-scale intermittency of the flow. Similar behaviour is characteristic of open flows. It was argued by Nicolaenko & She (1993) that such bursting phenomena in Kolmogorov flow are linked to the symmetry breaking of low-dimensional homoclinic cycles present in this flow.

3.3. *Transitional and low Reynolds number Kolmogorov flow*

Transitional and low Reynolds number Kolmogorov flows must be simulated using Newtonian viscosity and not hyperviscosity. In this case, it is useful to define the Reynolds number as

$$Re = \frac{F^{1/2}}{k_f^{3/2}\nu} \tag{3.16}$$

We find that transition to turbulence occurs at

$$Re_{crit} = 12\text{–}13 \tag{3.17}$$

corresponding to $\nu \approx 0.032$ for $F = 0.16$ and $k_f = 1$. Once the flow becomes turbulent the effective viscosity jumps to the value $\nu_{eff} = 0.14$ (see (3.8)), so there is an effective increase of friction coefficient at transition by about factor of 4. The details of the three-dimensional transition process for Kolmogorov flow may shed considerable light on transition in more complex flows. We performed a number of simulations of turbulent low Reynolds number Kolmogorov flows with Newtonian viscosity (up to Reynolds number $Re = 30$). In this range of Reynolds numbers the mean velocity profile and turbulence intensities still depend on the Reynolds number. Much larger numerical resolutions are required to reach the high Reynolds numbers that are accessible with the help of hyperviscosity at modest resolutions.

3.4. *Energy budget for Kolmogorov flow*

An important question in transport modelling of turbulence is the relative values of different terms in the energy balance equations. Assumptions are usually made about the relative importance of different terms in two-equation K–$\mathscr{E}$ transport models (Yakhot *et al.* 1992), and many of the terms in the energy budget are directly modelled in Reynolds stress models (Mansour, Kim & Moin 1988). The energy budget will also be important for the discussion of the local-isotropy hypothesis below. The balance equation for the $i = x, y, z$ component of velocity has the form

$$\frac{\mathrm{D}}{\mathrm{Dt}}\frac{\langle v_i' v_j' \rangle}{2} = P_{ij} + T_{ij} + D_{ij} + \Pi_{ij} + \mathscr{E}_{ij} \tag{3.18}$$

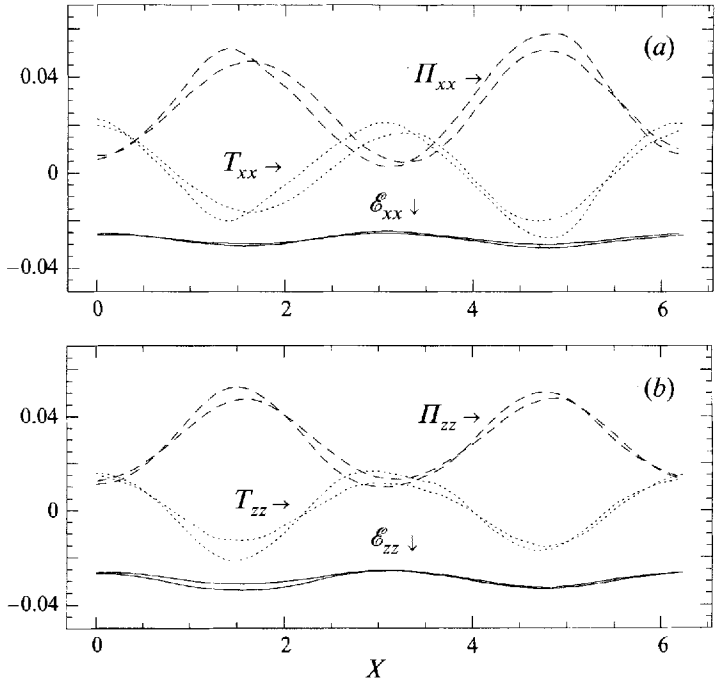

FIGURE 8. Terms in the budget of (*a*) $\langle u_x' u_x' \rangle$; (*b*) $\langle u_z' u_z' \rangle$. $\mathscr{E}_{xx}, \mathscr{E}_{zz}$ = dissipation rate (solid line); T_{xx}, T_{zz} = turbulent transport (dotted line); Π_{xx}, Π_{zz} = velocity–pressure gradient (dashed line). Measurements are performed for resolutions 128^3 and 64^3.

where $\mathrm{D}/\mathrm{D}t = \partial/\partial t + \langle v_k \rangle \, \partial/\partial x_k$ and

$$\left.\begin{aligned} P_{ij} &= -\frac{1}{2}\left[\langle v_i' v_k' \rangle \frac{\partial \langle v_j \rangle}{\partial x_k} + \langle v_j' v_k' \rangle \frac{\partial \langle v_i \rangle}{\partial x_k}\right], \\ \mathscr{E}_{ij} &= \nu_h \left\langle \Delta^{h/2} v_i' \Delta^{h/2} v_j' \right\rangle, \\ T_{ij} &= -\frac{1}{2} \frac{\partial \langle v_i' v_j' v_k' \rangle}{\partial x_k}, \\ \Pi_{i,j} &= -\frac{1}{2}\left\langle v_i' \frac{\partial p'}{\partial x_j} + v_j' \frac{\partial p'}{\partial x_i} \right\rangle. \end{aligned}\right\} \tag{3.19}$$

Following Mansour *et al.* (1988), the terms on the right-hand side of (3.19) are identified as follows: P_{ij} is the production rate, $\mathscr{E}_{ij}$ is the dissipation rate, T_{ij} is the turbulent transport rate, Π_{ij} is the velocity–pressure-gradient term and D_{ij} is the viscous diffusion rate. The primed velocities indicate their fluctuating parts. The explicit form of D_{ij} for hyperviscous dissipation is rather cumbersome. It turns out for the case of Kolmogorov flow that this term is smaller than the errors of our measurements so it may be neglected. In what follows we will discuss the budgets of equations (3.18) only for the case $i = j$.

In figures 8 and 9 we plot the terms (3.19) for the balance equation of each component of velocity and for the total turbulent kinetic energy. As may be seen,

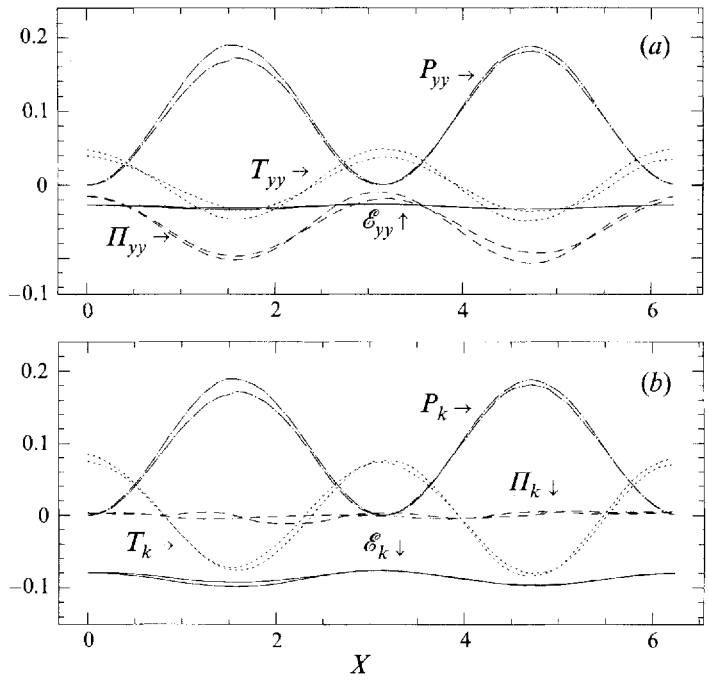

FIGURE 9. Terms in the budget of (*a*) $\langle u_y' u_y' \rangle$; (*b*) turbulent kinetic energy. $\mathscr{E}_{yy}, \mathscr{E}_k$ = dissipation rate (solid line); T_{yy}, T_k = turbulent transport (dotted line); Π_{yy}, Π_k = velocity pressure-gradient (dashed line). Measurements are performed for resolutions 128^3 and 64^3.

energy is input to the v_y-component of velocity by the force and then redistributed by pressure and turbulent transport to other components of velocity. All terms (3.19) have the very simple structure $a + b\cos(2x)$, where a and b are constants. The production of turbulence is inhomogeneous and the amplitude of the Π- and T-terms is quite large in comparison with the amplitude of the $\mathscr{E}$-term. The situation is similar to that for near-wall turbulence (Mansour *et al.* 1988) in which the role of the velocity pressure-gradient term is very important. It is interesting that, in the total energy balance equation, the velocity pressure-gradient term is nearly zero. Since pressure plays a major role in the local-in-space redistribution of energy among velocity components but not in the total energy balance, total energy is redistributed mostly by turbulent diffusion. It is worth noting that if the $T_k \approx 0.08\cos(2x)$ term in the total energy balance equation is interpreted as turbulent diffusion of K, we would obtain a nearly constant effective viscosity in the K-equation. It follows from (3.10) that the effective viscosity in this case is about 0.29 so that the effective turbulent 'Prandtl number' ≈ 0.5 (which is smaller than 0.72 given by RNG theory (Yakhot *et al.* 1992)).

A comparison of the energy balances at different Reynolds numbers reveals that the energy budget is practically independent of Reynolds number. We conclude that large-scale eddies are largely responsible for the redistribution of energy. This is a strong indication of the likelihood of existence of local-isotropy in Kolmogorov flow. In what follows we directly address the local isotropy hypothesis by studying correlation functions between the v_x- and v_y-components of the velocity and between v_y and the gradient of pressure $\partial_y p$, both of which should vanish in the isotropic case.

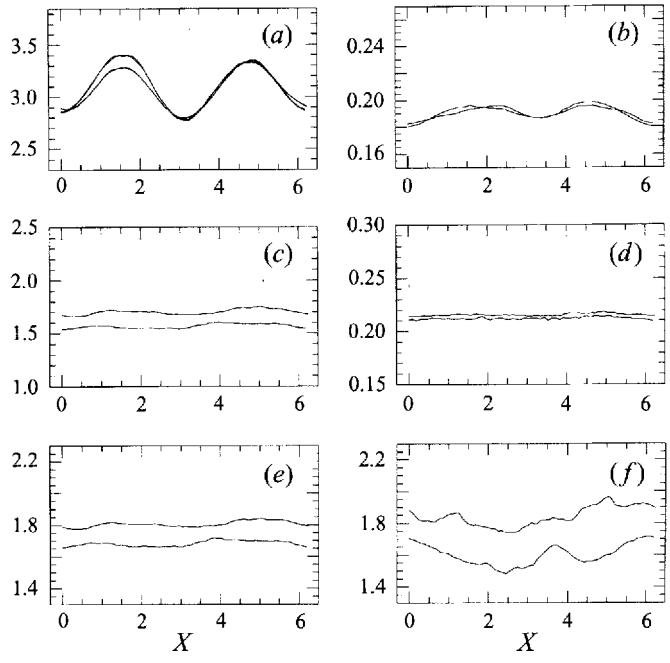

FIGURE 10. (*a*) $\langle S^2\rangle/(\bar{\mathscr{E}}k_d^{4/3})$ and $\frac{1}{2}\langle\omega^2\rangle/(\bar{\mathscr{E}}k_d^{4/3})$; (*b*) 'effective viscosity' $\langle\mathscr{E}\rangle k_d^{4/3}/(2\bar{\mathscr{E}}^{1/3}\langle S^2\rangle)$; (*c*) $\langle(S^2+0.5\omega^2)^2\rangle/\langle(S^2+0.5\omega^2)\rangle^2$; (*d*) $\langle(S^2-0.5\omega^2)^2\rangle/\langle(S^2+0.5\omega^2)^2\rangle$; (*e*) $\langle S^4\rangle/\langle S^2\rangle$; (*f*) $\langle\mathscr{E}^2\rangle/\langle\mathscr{E}\rangle$. Measurements are performed for resolutions 128^3: upper curves $k_d = 42$ and 64^3; lower curves $k_d = 21$.

In figure 10(*a*) the averages $\langle S^2 = S_{ij}S_{ij}\rangle$ and $\langle\frac{1}{2}(\omega^2 = \omega_i\omega_i)\rangle$ are plotted for numerical resolutions 64^3 and 128^3. We scale these quantities by $\bar{\mathscr{E}}^{2/3}k_d^{4/3}$ in accordance with Kolmogorov theory (1941), leading to their near collapse to one curve for different Reynolds numbers. Here $\bar{\mathscr{E}}$ is the energy dissipation rate averaged over the flow (including the x-direction). As was shown by Borue & Orszag (1995*a*), in the inertial range the statistical properties of the hyperviscous energy dissipation rate (2.4) are equivalent to those with 'renormalized' Newtonian effective viscosity (2.5), i.e. $\mathscr{E} = 2\nu_{eff}S^2$. To illustrate this idea we use (2.5) and our data to obtain the nearly constant 'renormalized' effective viscosity plotted in figure 10(*b*)

$$\nu_{eff} = \frac{\mathscr{E}}{2S^2} \approx 0.19\frac{\bar{\mathscr{E}}^{1/3}}{k_d^{4/3}}. \tag{3.20}$$

We also measured the higher-order quantities $\langle S^4\rangle$, $\langle\omega^4\rangle$, $\langle S^2\omega^2\rangle$ and $\langle\mathscr{E}^2\rangle$. In figure 10(*c*) we plot as an example the ratio $\langle(S^2+0.5\omega^2)^2\rangle/\langle(S^2+0.5\omega^2)\rangle^2$ that is one measure of intermittency. This ratio is a slowly growing function of Reynolds number. It is known that the pressure satisfies the equation $\Delta p = \omega^2/2 - S^2$. In figure 10(*d*) we plot the ratio $\langle(S^2-0.5\omega^2)^2\rangle/\langle(S^2+0.5\omega^2)^2\rangle$, which is nearly independent of Reynolds number and small. This demonstrates the strong negative small-scale correlation between S^2 and ω^2 as was noted in Borue & Orszag (1995*a*). If the energy dissipation rate were proportional to S^2 with nearly constant effective viscosity, we would expect that ratios $\langle S^4\rangle/\langle S^2\rangle^2$ and $\langle\mathscr{E}^2\rangle/\langle\mathscr{E}\rangle^2$ should behave similarly. This is indeed the case as illustrated in figure 10(*e,f*). An important conclusion of this

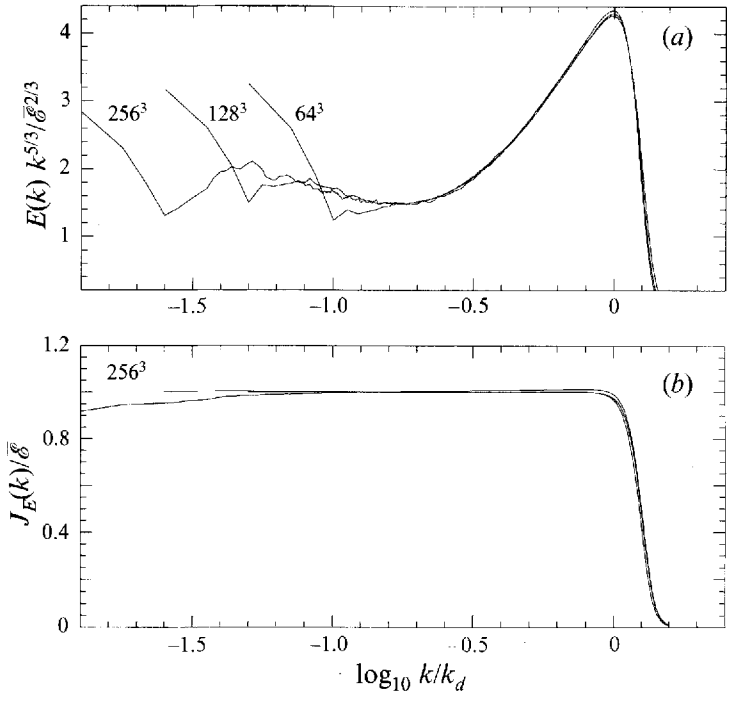

FIGURE 11. (*a*) Scaled isotropic energy spectra $E(k)k^{5/3}/\bar{\mathscr{E}}^{2/3}$ and (*b*) scaled energy fluxes $J_E(k)/\bar{\mathscr{E}}$ as functions of $log_{10}k/k_d$. Resolutions 256^3, 128^3 and 64^3 with $h = 8$.

analysis is that we have an indication that hyperviscosity leads effectively to constant renormalized 'normal' viscosity.

4. Local-isotropy hypothesis

Although Kolmogorov flow is anisotropic at large scales we begin our discussion with data for isotropic energy spectra (2.3) which are plotted in figure 11(*a*) as a function of $\log_{10} k/k_d$ for three different Reynolds numbers. As can be seen, these energy spectra collapse to one curve if k/k_d is large enough. There are also noticeable deviations from Kolmogorov's 5/3 law similar to those observed by Borue & Orszag (1995*a*). If the 5/3 law is assumed to hold, the Kolmogorov constant would be $C_K \approx 1.5$ (this value corresponds to the minimum of compensated energy spectrum in the inertial range). It is clear from figure 11(*b*) that the energy flux (see (2.2)) is nearly constant across a broad wavenumber range. For 256^3 numerical resolution, nearly two decades of constant energy flux is observed. We stress that this broad range of constant energy flux exists because we use hyperviscous dissipation. Nearly an order of magnitude higher numerical resolution in each direction would be required to obtain a similarly broad range of constant energy flux with Newtonian viscosity.

Near the dissipation cutoff k_d both isotropic and one-dimensional energy spectra have approximately half a decade in which $E(k)$ decays roughly as $1/k$ (see Borue & Orszag 1995*a*). This flattening of the energy spectra near k_d is termed the 'bottleneck' phenomenon (see Falkovich 1994 in which there is also a discussion of early theoretical works on this subject). As was shown by Borue & Orszag (1995*a*) the existence of the bottleneck is independent of the order h of hyperviscosity, but the range where the bottleneck is observed becomes slightly longer when higher order hyperviscosity

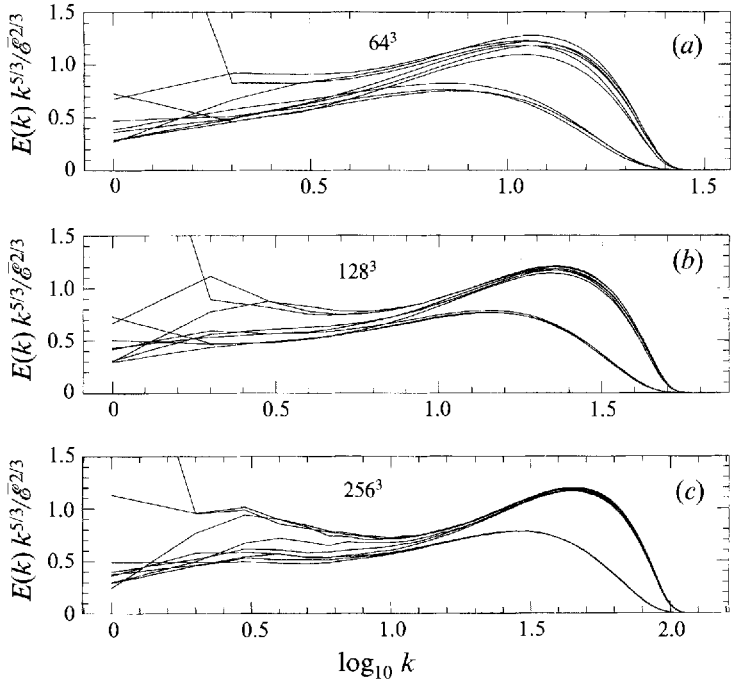

FIGURE 12. Nine one-dimensional energy spectra scaled by $k^{5/3}/\bar{\varepsilon}^{2/3}$ for three different resolutions: (*a*) 64^3; (*b*) 128^3; (*c*) 256^3.

is used. An increase of the bottleneck range visually corresponds to somewhat higher bumps in the compensated energy spectrum (see figure 11*a*) for higher-orders of hyperviscosity. The $1/k$ behaviour of the energy spectra near the dissipation cutoff was also reported by She & Jackson (1993) based on extrapolation of experimental data. A clear case of a bottleneck in energy spectra has been observed recently by Saddoughi & Veeravalli (1994) in their high Reynolds number experiments. It was also noted by Lohse & Müller-Groeling (1995) and by Sirovich, Smith & Yakhot (1994) that the Fourier transform of Batchelor's interpolation formula for the velocity structure function leads to a bottleneck-like energy spectrum. A similar bottleneck with $1/k$ scaling was observed recently in numerical simulations of compressible turbulence by Porter *et al.* (1992). Some indications of the existence of a bottleneck in energy spectra was found in numerical simulations of incompressible homogeneous turbulence by Vincent & Meneguzzi (1991) and by She *et al.* (1993). Unfortunately, with Newtonian viscosity, this bottleneck region is not fully resolved even using 512^3 resolution. In our recent work (Borue & Orszag 1995*a*) we have presented some evidence that the bottleneck in energy spectra is due to a sharp and rapid change of the energy transfer mechanism near the dissipation cutoff. A qualitative explanation of the bottleneck in the energy spectrum may be based on the similarity of the energy transfer mechanism near k_d to that of a passive scalar undergoing large-scale straining of small-scale fields which also leads to a k^{-1} spectrum (Batchelor 1959) independent of the space dimension (Kraichnan 1974).

4.1. *Local isotropy of one-dimensional energy spectra*

To analyse the local isotropy of Kolmogorov flow we measure all nine one-dimensional energy spectra defined by (2.10), which are plotted in figure 12(*a–c*) for different

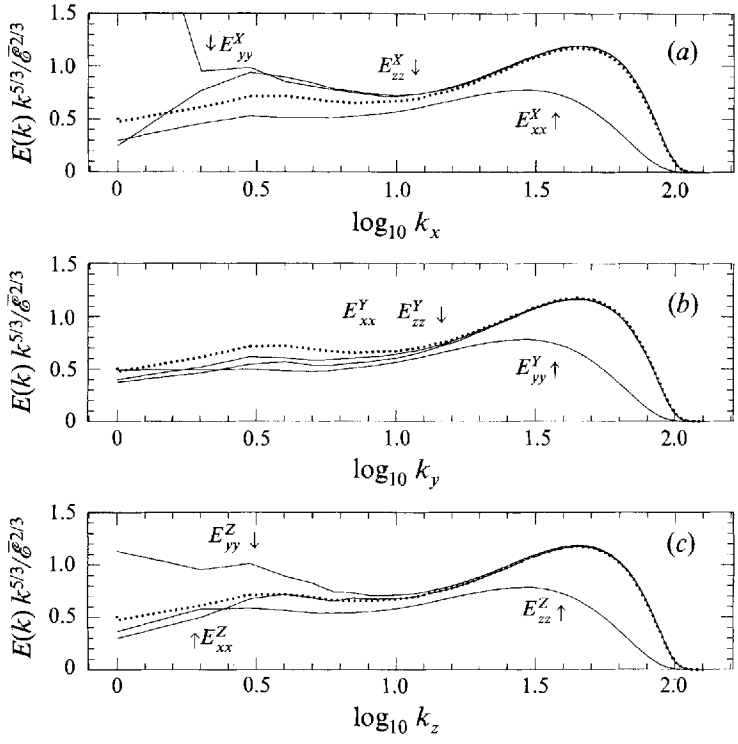

FIGURE 13. One-dimensional energy spectra scaled by $k^{5/3}/\bar{\mathscr{E}}^{2/3}$ as a function of $\log_{10} k$. The hyperviscous run with resolution 256^3 is used. The dotted lines are transverse spectra calculated from longitudinal ones according to (2.11) and scaled by $k^{5/3}/\bar{\mathscr{E}}^{2/3}$. (*a*) $E^X_{xx}, E^X_{yy}, E^X_{zz}$; (*b*) $E^Y_{xx}, E^Y_{yy}, E^Y_{zz}$; (*c*) $E^Z_{xx}, E^Z_{yy}, E^Z_{zz}$.

Reynolds numbers. The spectra are scaled by $k^{5/3}/\bar{\mathscr{E}}^{2/3}$. Obviously for locally isotropic flow all three longitudinal and all six transverse spectra should coincide with each other. As may be seen, that is not the case. For 64^3 resolution these spectra are different well into the dissipation range. However, for the higher Reynolds numbers runs with 128^3 and in particular 256^3 resolution, the spectra nearly coincide starting from wavenumbers ≈ 20.

In figure 13(*a–c*) we study local isotropy for the 256^3 run in more detail. One-dimensional spectra of the three components of velocity are plotted in figure 13(*a*,*b*,*c*) for measurements along the (x, y, z)-directions, respectively. All energy spectra are scaled by $k^{5/3}/\bar{\mathscr{E}}^{2/3}$. The dotted curves in the figures are transverse spectra calculated from the corresponding longitudinal ones according to (2.11). These results show that local isotropy is established at wavenumbers starting from $k \approx 10$–20.

There are substantial differences between one-dimensional spectra measured along and across Kolmogorov flow. Spectra measured along the mean flow (y-direction) follow closely the Kolmogorov law, while transverse spectra in the x- and z-directions deviate substantially from Kolmogorov's law. In fact, the scaling law of the E^X_{zz}, E^X_{yy} spectra of the v_y, v_z-components of velocity measured in the x-direction and the E^Z_{yy} spectra of v_y measured in the z-direction are quite close to $1/k^2$. This $1/k^2$ law may indicate formation of strong vortex sheets or high gradients of velocity.

Kolmogorov flow is a shear flow which may be characterized by its mean shear $\langle S_{yx} \rangle$ and mean dissipation rate $\bar{\mathscr{E}}$. As was suggested by Lumley (1967) (see also

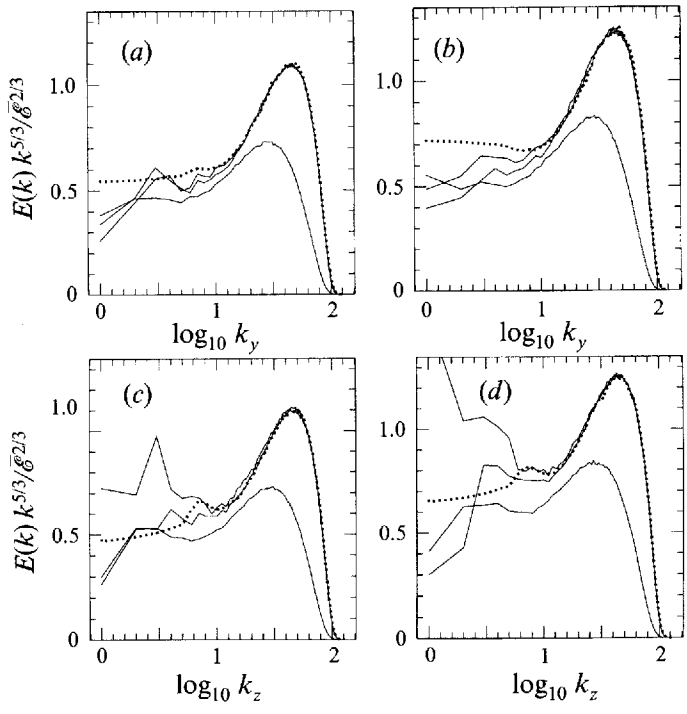

FIGURE 14. One-dimensional energy spectra scaled by $k^{5/3}/\bar{\mathscr{E}}^{2/3}$ as a function of $\log_{10} k$. The hyperviscous run with resolution 256^3 is used. The dotted lines are transverse energy spectra calculated from longitudinal ones according to (2.11) and scaled by $k^{5/3}/\bar{\mathscr{E}}^{2/3}$. The spectra (*a*), (*c*) are measured in low-strain regions, and the spectra (*b*), (*d*) are measured in high-strain regions. (*a*), (*b*) $E^Y_{xx}, E^Y_{yy}, E^Y_{zz}$; (*c*), (*d*) $E^Z_{xx}, E^Z_{yy}, E^Z_{zz}$.

Yakhot 1994 and Saddoughi & Veeravalli 1994) the dimensionless parameter that characterizes the relative importance of shear is $\langle S\rangle/(\bar{\mathscr{E}}^{1/3}k^{2/3})$. Therefore, mean shear should be unimportant for wavenumbers satisfying

$$k > k_s = C_s \frac{\langle S\rangle^{3/2}}{\bar{\mathscr{E}}^{1/2}} \tag{4.1}$$

where C_s is some numerical constant. It follows from the experimental data obtained by Saddoughi & Veeravalli (1994) that the constant here is $C_s \approx 10$. Thus, the wavenumber of the onset of local isotropy k_s should depend only on the local mean shear $\langle S\rangle$.

We can test these ideas in Kolmogorov flow where the mean shear varies from zero to one. It is natural then to suggest that anisotropy will be maximal at x-locations where the mean shear is maximal and local isotropy will be maximal at x-locations where the mean shear equals zero. In figures 12 and 13 we show one-dimensional energy spectra averaged over the x-direction only. In figure 14 we plot one-dimensional energy spectra measured in the y ($E^Y_{xx}, E^Y_{yy}, E^Y_{zz}$) and the z ($E^Z_{xx}, E^Z_{yy}, E^Z_{zz}$) directions, but here the measurements are carried out first at points where $\langle S\rangle \approx 0$ and then at points where $|\langle S\rangle|$ is maximal. As may be seen from these results, local isotropy is a good approximation to these spectra starting from approximately the same wavenumber $k_s \approx 15$ independently of whether the regions have high or low shear. Thus, the onset of local isotropy seems to be a global property of turbulence at least for such large-scale intermittent open systems as Kolmogorov flow. The reason for this violation of

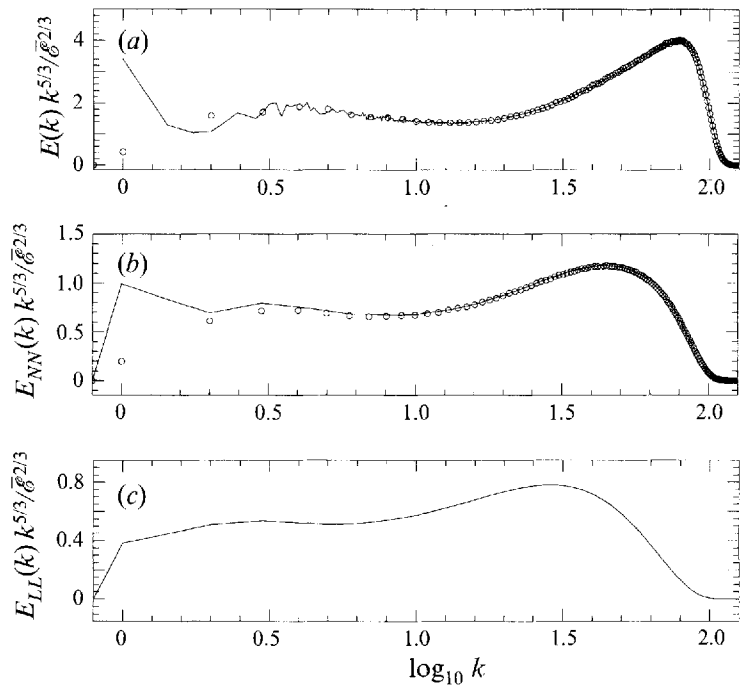

FIGURE 15. (*a*) Isotropic energy spectrum, (*b*) transverse energy spectrum and (*c*) longitudinal energy spectrum as functions of $\log_{10} k$. The resolution is 256^3. All spectra are scaled by $k^{5/3}/\bar{\mathscr{E}}^{2/3}$. Points are the isotropic energy spectrum calculated from the transverse and longitudinal energy spectra and the transverse energy spectrum calculated from the longitudinal energy spectrum according to (2.11) and (2.12).

(4.1) may be that although the mean strain is zero in some regions of the flow the fluctuating part of the strain is not negligible compared to that of the mean strain. If we estimate C_s using the absolute value of the mean shear averaged over x we would conclude that $C_s \approx 9$ in reasonable agreement with Saddoughi & Veeravalli (1994).

There is an interesting feature of the observed large-scale anisotropy of Kolmogorov flow. If we disregard anisotropy, we may simply obtain the 'isotropic' longitudinal spectrum by averaging the three individual longitudinal spectra and similarly obtain the 'isotropic' transverse spectrum by averaging the six individual transverse spectra. Then we may calculate the transverse spectrum E_{NN} from the longitudinal one using (2.11) and compare it with the measured spectrum. We may also calculate the isotropic energy spectrum using (2.12) and compare it with the directly measured isotropic energy spectrum. The results of these calculations are shown in figure 15. As may be seen these 'isotropic' spectra satisfy local isotropy starting from nearly the lowest wavenumber: an increase of fluctuations of the y- and z-components of velocity is approximately compensated by a corresponding decrease of fluctuations of the x-component of velocity. We have not performed a systematic study of the energy spectra anisotropy in three-dimensional wavenumber space. But we think that this cancellation of anisotropic contributions to the energy spectra might be an indication that energy spectra are sums of isotropic and anisotropic contributions. The anisotropic contributions, which decay faster than isotropic ones, cancel out when summed over different components of velocity. Thus pressure can play a major role in restoring local isotropy by redistributing energy between different components of the velocity (see §3.4).

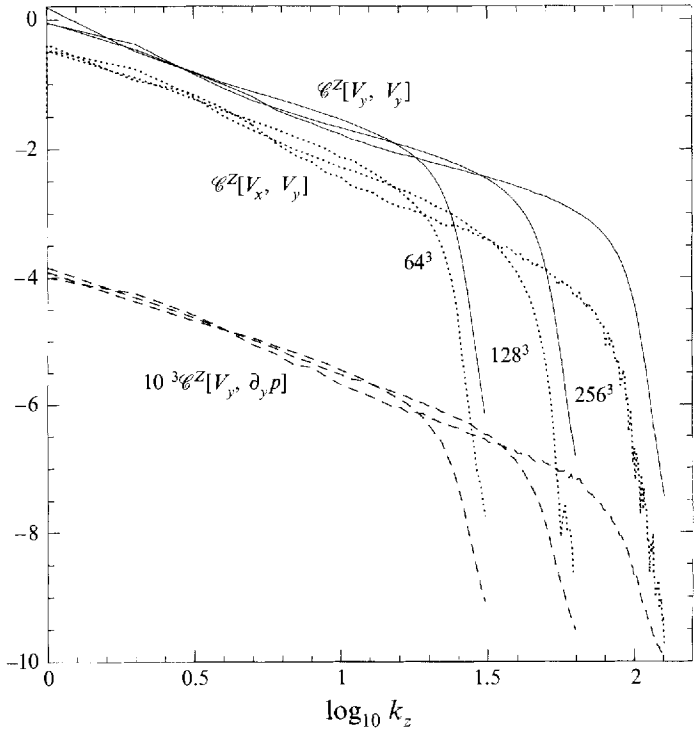

FIGURE 16. $\mathrm{Log}_{10} - \log_{10}$ plots of one-dimensional transverse energy spectra $\mathscr{C}^Z[v_y, v_y]/\bar{\mathscr{E}}^{2/3}$ (solid lines), one-dimensional cross-spectra $\mathscr{C}^Z[v_x, v_y]/\bar{\mathscr{E}}^{2/3}$ (dotted lines), one-dimensional velocity pressure-gradient cross-spectra $\mathscr{C}^Z[v_y, \partial_y p]/(1000\bar{\mathscr{E}})$ (dashed lines). The spectra are measured in the z-direction and are plotted for three numerical resolutions: 64^3, 128^3 and 256^3.

4.2. *Algebraic decay of anisotropic spectra*

At high Reynolds numbers, we have demonstrated that local isotropy holds at sufficiently large wavenumbers, but the establishment of local isotropy occurs rather slowly with increasing k. As argued by Nelkin & Nakano (1983), anisotropy should decay slower than $1/k^{2/3}$.

Following Saddoughi & Veeravalli (1994) we measure the cross-spectrum between the v_x- and v_y-components of velocity density $\mathscr{C}^\alpha[v_x, v_y]$ defined in (2.13) for $\alpha = Y, Z$. Another correlation that characterizes anisotropy is the correlation between velocity and pressure gradient $\mathscr{C}^\alpha[v_y \partial_y p]$ for $\alpha = Y, Z$. Both of these correlation functions should equal zero in isotropic flows. As was shown in §§3.1 and 3.4 both $\langle v_x v_y \rangle$ and $\langle v_y \partial_y p \rangle$ are not equal to zero and are functions of x. Averaged in the x-direction the correlation $\langle v_x v_y \rangle$ equals zero while the correlation $\langle v_y \partial_y p \rangle$ is non-zero even when averaged over x.

We first check that, when measured at a given space point x in the directions $\alpha = Y, Z$ the correlation $\mathscr{C}^\alpha[v_x, v_y](k_\alpha)$ behaves as $\langle S(x) \rangle f(k_\alpha)$. Thus it changes sign when $\langle S(x) \rangle$ changes sign. We perform our measurements at locations x where the stress is maximal in absolute value. To increase our statistical database we measure the spectral density of $\mathscr{C}^\alpha[v_y, \partial_y p](k_\alpha)$ with an additional averaging over the x-direction. The $\log_{10} - \log_{10}$ plots of these spectral correlations along with one-dimensional energy spectra are shown in figure 16 (where all spectra are scaled by an appropriate power of $\bar{\mathscr{E}}$ and the spectra of $\mathscr{C}^\alpha[v_y, \partial_y p](k_\alpha)$ are artificially rescaled

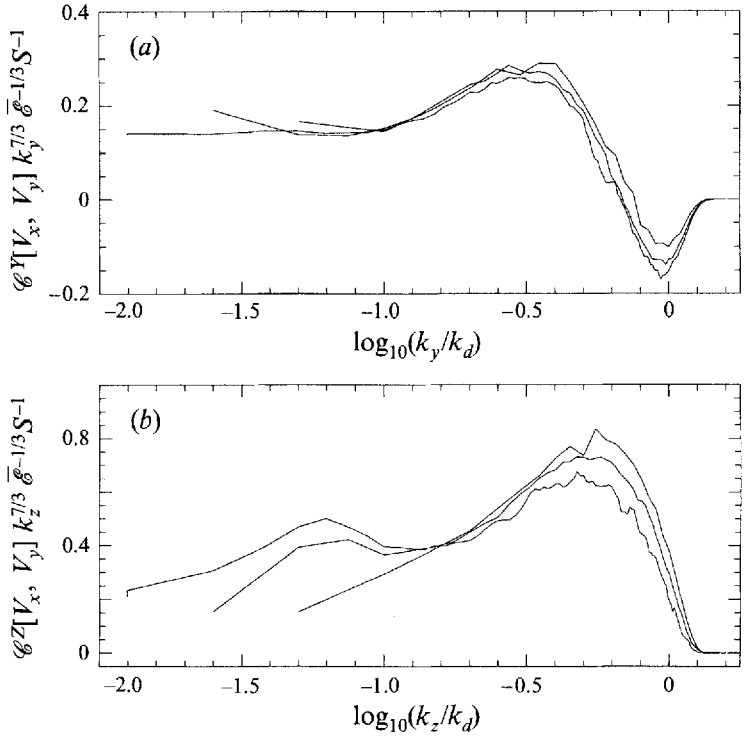

FIGURE 17. One-dimensional cross-spectra $\mathscr{C}^\alpha[v_x, v_y]/(\bar{\mathscr{E}}^{1/3}\langle S\rangle)$ scaled by $k^{7/3}$ as a function of $\log_{10} k/k_d$ for numerical resolutions 64^3, 128^3 and 256^3. Measurements are performed in high-shear regions. (*a*) Spectra in the $\alpha = Y$ direction; (*b*) spectra in the $\alpha = Z$ direction.

by a factor of 1000). It is interesting that the cross-spectral correlations are non-zero and scale algebraically even at those wavenumbers where we observe local isotropy on the level of one-dimensional energy spectra.

It is expected from Lumley (1967), Yakhot (1994), Grossman *et al.* (1994) that the shear-stress co-spectrum should scale linearly with $\langle S\rangle$ as

$$\mathscr{C}^\alpha[v_x, v_y](k) = C_0 \frac{\bar{\mathscr{E}}^{1/3}\langle S\rangle}{k^{7/3}}. \tag{4.2}$$

In figure 17(*a*,*b*) we scale $\mathscr{C}^\alpha[v_x, v_y](k)$ by $k^{7/3}/(\bar{\mathscr{E}}^{1/3}\langle S\rangle)$. It may be seen that our data agree reasonably well with (4.2). The one-dimensional co-spectra measured in the y-direction show better scaling than co-spectra measured in the z-direction. The constant $C_0 = 0.2 - 0.4$. In figure 18(*a*,*b*) we also plot the correlation, coefficient spectrum defined in (2.14); it algebraically decreases from 0.6 to zero and even negative values.

In figure 19(*a*–*c*) we plot velocity–pressure-gradient co-spectra $\mathscr{C}^\alpha[v_y, \partial_y p](k_\alpha)$ measured in the $\alpha = (X, Y, Z)$-directions. These co-spectra are scaled by $k^2/\bar{\mathscr{E}}$ and thus have the form

$$\mathscr{C}^\alpha[v_y, \partial_y p](k) \approx 0.2 \frac{\bar{\mathscr{E}} k_f}{k^2} \tag{4.3}$$

where $k_f = 1$ is the scale of the force. Naively we would expect Kolmogorov-like scaling for this correlator as $\bar{\mathscr{E}}/k$. Thus the anisotropy decays in this case as $1/k$, even faster than $1/k^{2/3}$.

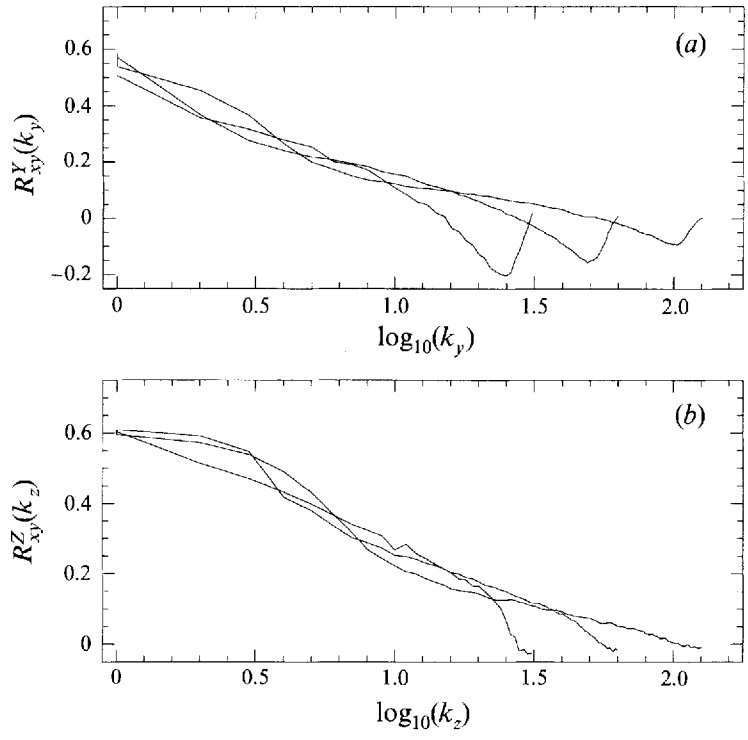

FIGURE 18. One-dimensional correlation-coefficient spectra R^{α}_{xy} as a function of $\log_{10} k$ for numerical resolutions 64^3, 128^3 and 256^3. (*a*) Spectra in the $\alpha = Y$ direction; (*b*) spectra in the $\alpha = Z$ direction.

Therefore anisotropy in co-spectra decays algebraically and relatively slowly in accordance with the predictions of Nelkin & Nakano (1983). We think that such a slow decay may have significant dynamical consequences for Navier–Stokes turbulence.

There are also spectra that are rather insensitive to large-scale anisotropy. An example is the spectrum of the energy dissipation rate correlation function. The energy dissipation rate is defined according to (2.4). The scaling of the spectrum of energy dissipation rate $\mathscr{C}^{\alpha}[\mathscr{E},\mathscr{E}] \sim 1/k^{1-\mu}$ defines the so-called intermittency exponent μ. According to the recent work of Sreenivasan & Kailasnath (1993), $\mu \approx 0.25 \pm 0.05$. We have checked that the spectrum of energy dissipation rate is locally isotropic and has the form

$$\mathscr{C}^{\alpha}[\mathscr{E},\mathscr{E}](k) \approx 0.15 \frac{\bar{\mathscr{E}}^2}{k^{1-\mu} k_f^{\mu}} \tag{4.4}$$

with $\mu \approx 0.22$ (see figure 20). This scaling is consistent both with Sreenivasan & Kailasnath (1993) and with the results of Borue & Orszag (1995*a*).

4.3. *Anisotropy of vorticity skewness*

One of the important dynamical consequences of the slow decay of anisotropy may be the persistent small-scale anisotropy of higher-order moments. It was recently noticed by Pumir & Shraiman (1995) that in homogeneous shear flows the skewness of the z-component of vorticity ω_z,

$$\gamma_1^{\omega} = \mu_3(\omega_z)/\sigma^3(\omega_z), \tag{4.5}$$

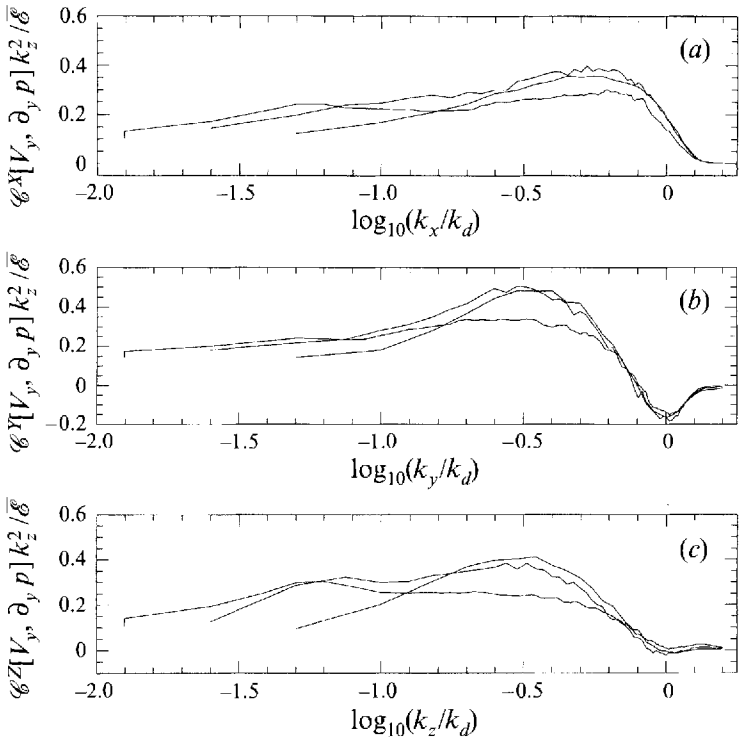

FIGURE 19. One-dimensional velocity–pressure-gradient cross-spectra $\mathscr{C}^{\alpha}[v_y, \partial_y p]/\bar{\mathscr{E}}$ scaled by k^2 as a function of $\log_{10}(k/k_d)$ for numerical resolutions 64^3, 128^3 and 256^3. Spectra are averaged over the flow in x-direction. (*a*) Spectra in the $\alpha = X$ direction; (*b*) spectra in the $\alpha = Y$ direction; (*c*) spectra in the $\alpha = Z$ direction.

is independent of Reynolds number and $\gamma_1^{\omega} \approx -0.53$. Here $\mu_n(\omega_z)$ is the nth order central moment and $\sigma(\omega_z)$ is the variance of ω_z. In the case considered by Pumir & Shraiman (1995) ω_z was the only component of vorticity with non-zero negative mean that was constant in space. That is, the small-scale vorticity was more skewed in the direction of the mean large-scale vorticity. Obviously, for locally isotropic turbulence, vorticity skewness should vanish.

It is interesting to check this remarkable result for Kolmogorov flow, i.e. for inhomogeneous shear flow. In the case of Kolmogorov flow, ω_z is also the only vorticity component with non-zero mean. To perform this calculation we use low-pass spatial isotropic filters φ_ℓ of scale ℓ defined for any quantity $A(x)$ as

$$A^{(\ell)}(x) = \int \varphi_\ell(x-y)A(y)\mathrm{d}^3y \tag{4.6}$$

and normalized $\int \varphi_\ell(x)\mathrm{d}^3x = 1$. In Fourier space $\varphi_\ell(\boldsymbol{k}) = \exp(-\xi^8)$ with $\xi = \ell|\boldsymbol{k}|$. We check that the results are insensitive to the form of filter used. We measure the joint probability distribution $\mathscr{P}(\tilde{v}_{yx}, \omega_z^{(\ell)})$, where $\tilde{v}_{yx} = \partial_x v_y^{(\ell)}$ with $\ell = 1/2$ is shear filtered at large scales and $\omega_z^{(\ell)}$ is the small-scale vorticity, filtered at inertial range scales with $\ell = 1/8, 1/16, 1/32$ (see (4.6)). The conditional vorticity skewness $\gamma_1^{\omega}(\tilde{v}_{yx})$ is defined using (4.5) but the moments of $\omega_z^{(\ell)}$ are conditioned on the large-scale shear $\tilde{v}_{yx}$. The results for $\gamma_1^{\omega}(\tilde{v}_{yx})$ are plotted in figure 21 for 64^3 and 128^3 resolution. As can be seen, the functions $\gamma_1^{\omega}(\tilde{v}_{yx})$ are nearly independent of ℓ and Reynolds number and depend

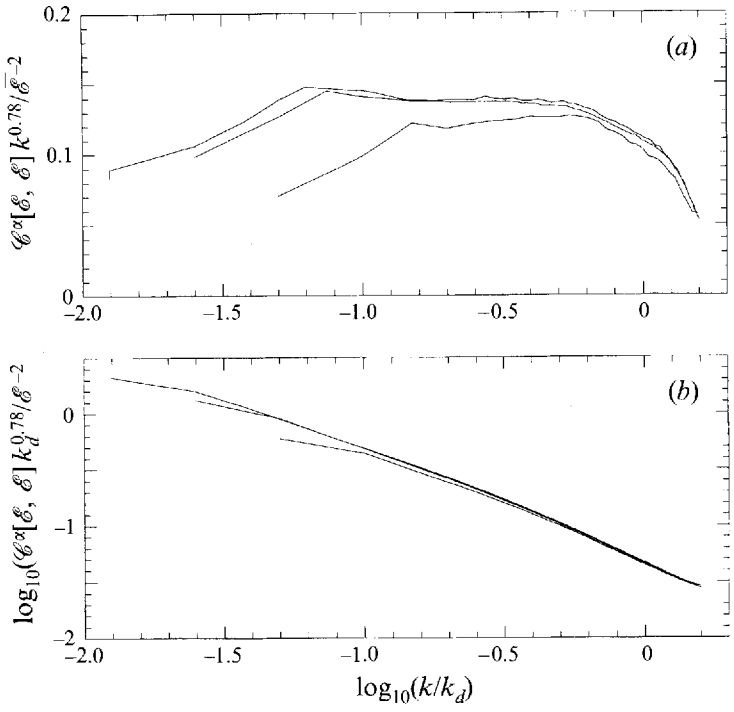

FIGURE 20. One-dimensional energy dissipation rate spectra $\mathscr{C}^{\alpha}[\mathscr{E},\mathscr{E}]/\bar{\mathscr{E}}^2$ as a function of $\log_{10}(k/k_d)$ for numerical resolutions 64^3, 128^3 and 256^3. (*a*) Spectra scaled by k^{γ}; (*b*) $\log_{10}$ of spectra multiplied by k_d^{γ} with $\gamma = 0.78$. Spectra are averaged over the flow and in all three $\alpha = X, Y, Z$ directions.

linearly on the large-scale shear $\tilde{v}_{yx}$. In regions of large $|\tilde{v}_{yx}|$, the vorticity skewness $|\gamma_1^{\omega}| \approx 0.5$ with the sign of skewness determined by the direction of the large-scale vorticity. These results are consistent with the case of homogeneous shear considered by Pumir & Shraiman (1995).

Thus, violations of local isotropy for higher-order moments may coexist with locally isotropic second-order moments. The non-zero value of vorticity skewness reflects the large-scale anisotropy and its probably non-universal value varies in space synchronously with the isotropy-breaking large-scale shear. This is a direct indication that the statistics of higher-order moments may be non-universal and sensitive to a large-scale structure of a flow. We think that anisotropic structures (such as vortex sheets or tubes) may play an important role in violations of local isotropy. These structures have large scale size in some directions and small scale size in other directions. It may be natural to expect that these structures are oriented by large-scale anisotropy thus leading to small-scale anisotropy.

5. Discussion

One result is the demonstration of the advantages of using hyperviscosity to simulate high Reynolds number turbulence. In itself, replacing Newtonian dissipation by hyperviscous dissipation is a serious test of Kolmogorov's universality ideas. In fact, as we found earlier (Borue & Orszag 1995*a*,*b*), we again have an indication that three-dimensional inertial-range dynamics may be relatively independent of the particular mechanism of small-scale dissipation. In addition, as in our early work,

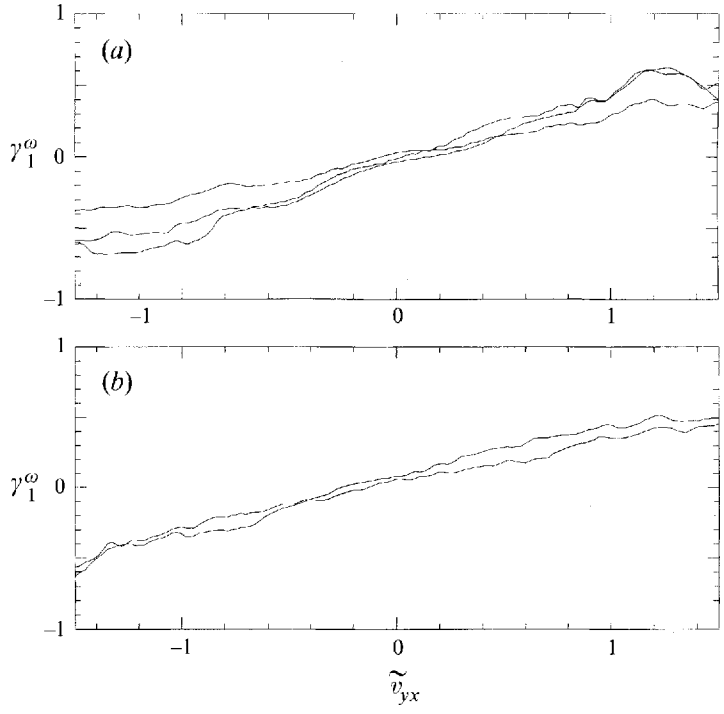

FIGURE 21. Conditional vorticity skewness $\gamma_1^\omega(\tilde{v}_{yx})$ for filtered vorticity component $\omega_z^{(\ell)}$ as a function of large-scale shear $\tilde{v}_{yx}$. (*a*) Numerical resolution is 128^3 and filter sizes are $\ell = 1/8, 1/16, 1/32$. (*b*) Numerical resolution is 64^3 and filter sizes are $\ell = 1/8, 1/16$.

there is also indication that the low-order statistics of energy dissipation fluctuations is independent of the form of energy dissipation. In contrast, our results have shown that the dynamics is strongly influenced by the mechanism of forcing.

In forced homogeneous turbulence, we have observed (Borue & Orszag 1995*a*) a deviation from the Kolmogorov 5/3 law, namely $E(k) \sim 1/k^{1.85}$. On the other hand, for freely decaying homogeneous turbulence, the 5/3 law seems to hold. We have found here that Kolmogorov flow is anisotropic at large scales with strong deviations of some transverse velocity correlation functions from the Kolmogorov 5/3 law. This may shed light on our earlier results for hyperviscous homogeneous turbulence, as white-in-time large-scale forcing will set up large-scale anisotropy, as in Kolmogorov flow, for a few large-eddy turnover times. After long time though, statistical isotropy of the flow will be fully recovered by the isotropic white-noise forcing: orientations of the large-scale anisotropic flow will slowly change in time. The fact that for several large-eddy turnover times there is large-scale anisotropy reveals itself in deviations from the Kolmogorov law. The observed $1/k^2$ scaling of some components of the energy spectrum in Kolmogorov flow is smeared out and perhaps contaminates the isotropic energy spectrum leading to the $E(k) \sim 1/k^{1.85}$ result. However, it is possible that the observed anomalous scaling is a true high Reynolds number effect.

Most measurements of energy spectra in the laboratory are done using Taylor's hypothesis in conjunction with measurements of correlation functions along the mean flow. Often mean flows have quite noticeable shear with $\eta \approx 2 - 6$. Here, we have shown that properties of correlation functions along and across the flow are quite different. In fact, energy spectra measured along the flow demonstrate a clear tendency

towards Kolmogorov scaling in contrast to correlation functions measured across the flow. In only a few laboratory experiments has local isotropy even been checked along the flow and we are not aware of any verification of the local-isotropy hypothesis involving measurements of correlation functions across the flow.

We have also shown that even for large-scale anisotropic flow, local isotropy is recovered with increasing Reynolds number but with an algebraically slow decay of anisotropic corrections. This slow decay of anisotropy may lead to anisotropy of higher-order moments even when local isotropy is recovered for second-order moments. Thus our results confirm the local-isotropy hypothesis at least for low-order moments. It is worthwhile mentioning that although the local-isotropy hypothesis also holds within the hyperviscous dissipation range, properties of this dissipation range should depend on the form of hyperviscosity. The lower wavenumber limit of locally isotropic behaviour in Kolmogorov flow seems to be a global property of the flow and not a function of only the local mean shear rate as in Saddoughi & Veeravalli (1994). Although the criteria (4.1) for onset of local isotropy still can be used, $\langle S \rangle$ should be replaced by the r.m.s. value of large-scale strain. This global character of the onset of local isotropy is likely due to the intermittent behaviour of Kolmogorov flow even at large scales.

Another conclusion is that Kolmogorov flow may be an ideal environment for testing of turbulence transport models. There are no walls in this flow, eliminating complications connected with boundary layers. The level of turbulence intensity is high. However, the large-scale intermittency of Kolmogorov flow makes this flow difficult to model and perhaps similar to open flows like jets and wakes. On the other hand, the simple structure of its mean flow characteristics may make Kolmogorov flow simple enough to attempt analytic theory.

We have shown that the standard expression for effective viscosity used in turbulence transport approximations should be modified to account for the time-dependent character of the flow. Indeed C_μ becomes a nearly linearly decreasing function of the dimensionless shear η. These results are consistent with the theoretical predictions of Smith & Yakhot (1993). Further work is needed to systematically study various approximations used in turbulence transport models.

We are grateful to V. Yakhot, K. Sreenivasan and I. Staroselsky for valuable discussions and to B. Shraiman for providing his work prior to publication. The computations have been performed on the Intel Delta at Caltech and on the IBM PVS at Princeton. This work was supported by ARPA and ONR under Contracts N00014-92-J-1796 and N00014-93-C-0216.

REFERENCES

BARTELLO, P., METAIS, O. & LESIEUR, M. 1994 Coherent structures in rotating three-dimensional turbulence. *J. Fluid Mech.* **273**, 1–29.

BATCHELOR, G. K. 1959 Small-scale variation of convected quantities like temperature in turbulent fluid. *J. Fluid Mech.* **5**, 113–133.

BORUE, V. 1993 Spectral exponent of enstrophy cascade in stationary two-dimensional homogeneous turbulence. *Phys. Rev. Lett.* **71**, 3967–3970.

BORUE, V. & ORSZAG, S. 1995*a* Forced three-dimensional homogeneous turbulence with hyperviscosity. *Europhys. Lett.* **29**, 687–692.

BORUE, V. & ORSZAG, S. 1995*b* Self-similar decay of three-dimensional homogeneous turbulence with hyperviscosity. *Phys. Rev.* E **52**, R856–859.

BRASSEUR, J. G. & WEI, C.-H. 1994 Interscale dynamics and local isotropy in high Reynolds number turbulence within triadic interaction. *Phys. Fluids* **6**, 842–870.

CAZALBOU, J. B. & BRADSHAW, P. 1993 Turbulent transport in wall bounded flows. Evaluation of model coefficients using direct numerical simulations. *Phys. Fluids* A **5**, 3233–3239.

E, WEINAN & SHU C.-W. 1993 Effective equations and the inverse cascade theory for Kolmogorov flows. *Phys. Fluids* A **5**, 998–1010.

FALKOVICH, G. 1994 Bottleneck phenomenon in developed turbulence. *Phys. Fluids* **6**, 1411.

GROSSMANN, S., LOHSE, D., LVOV, V. & PROCACCIA, I. 1994 Finite size corrections to scaling in high Reynolds number turbulence. *Phys. Rev. Lett.* **73**, 432–435.

HERRING, J. R. & METAIS, O. 1989 Numerical experiments in forced stably stratified turbulence. *J. Fluid Mech.* **202**, 97–115.

JACKSON, E., SHE, Z.-S. & ORSZAG, S. A. 1991 A case study in parallel computing: I. homogeneous turbulence on a hypercube. *J. Sci. Comput.* **6**, 27–45.

KOLMOGOROV, A. N. 1941 The local structure of turbulence in incompressible viscous fluid at high Reynolds number. *CR Acad. Sci. URSS* **30**, 301.

KOLMOGOROV, A. N. 1962 A refinement of previous hypotheses concerning the local structure of turbulence in a viscous incompressible fluid at high Reynolds number. *J. Fluid Mech.* **13**, 82–85.

KRAICHNAN, R. 1974 Convection of a passive scalar by a quasi-uniform random straining field. *J. Fluid Mech.* **64**, 737–762.

LOHSE, D. & MÜLLER-GROELING, A. 1995 Bottleneck effects: scaling phenomena in r- versus p-space. *Phys. Rev. Lett.* **74**, 1747–1750.

LUMLEY, J. L. 1967 Similarity and the turbulent energy spectrum. *Phys. Fluids* **10**, 855–858.

MANSOUR, N. N. KIM, J. & MOIN, P. 1988 Reynolds-stress and dissipation-rate budgets in a turbulent channel flow. *J. Fluid Mech.* **194**, 15–44.

MESHALKIN, L. D. & SINAI, Y. G. 1961 Investigations of the stability of a stationary solution of a system of equations for the plane movement of an incompressible viscous liquid *J. Appl. Maths* **25**, 1140–1143.

MONIN, A. S. & YAGLOM, A. M. 1975 *Statistical Fluid Mechanics*, vol. 2. MIT Press.

NELKIN, M. & NAKANO, T. 1983 How do the small scales become isotropic in Navier–Stokes turbulence. In *Turbulence and Chaotic Phenomena in Fluids* (ed. T. Tatsumi), p. 319. Elsevier.

NICOLAENKO, B. & SHE, Z.-S. 1993 Turbulent bursts, inertial sets and symmetry-breaking homoclinic cycles in periodic Navier–Stokes flows. In *Turbulence in Fluid Flows* (ed. G. R. Sell *et al.*), pp. 123–136. Springer.

PORTER, D. H., POUQUET, A. & WOODWARD, P. R. 1992 Three-dimensional supersonic homogeneous turbulence: a numerical study. *Phys. Rev. Lett.* **68**, 3156–3159.

PUMIR, A. & SHRAIMAN B. I. 1995 Persistent small scale anisotropy in homogeneous shear flows. *Phys. Rev. Lett.* to appear.

SADDOUGHI, S. G. & VEERAVALLI, S. V. 1994 Local isotropy in turbulent boundary layers at high Reynolds number. *J. Fluid Mech.* **268**, 333–372.

SHE, Z.-S., CHEN, S., DOOLEN, G., KRAICHNAN, R. H. & ORSZAG, S. A. 1993 Reynolds number dependence of isotropic Navier-Stokes turbulence. *Phys. Rev. Lett.* **70**, 3251–3254.

SHE, Z.-S. & JACKSON, E. 1993 On the universal form of energy spectra in fully developed turbulence. *Phys. Fluids* A **5**, 1526–1528.

SIROVICH, L., SMITH, L. & YAKHOT, V. 1994 Energy spectrum of homogeneous and isotropic turbulence in far dissipation range. *Phys. Rev. lett.* **72**, 344–347.

SMITH, L. & YAKHOT, V. 1993 Short and long-time behaviour of eddy viscosity models. *Theor. Comput. Fluid Dyn.* **4**, 197–217.

SREENIVASAN, K. R. 1991 On local isotropy of passive scalars in turbulent shear flows. *Proc. R. Soc. Lond.* A **434**, 165–182.

SREENIVASAN, K. R. & KAILASNATH, P. 1993 An update on the intermittency exponent in turbulence. *Phys. Fluids* A **5**, 512–514.

SULEM, P. L., SHE, Z.-S., SCHOLL, H. & FRISH, U. 1989 Generation of large-scale structures in the three-dimensional flow lacking parity-invariance. *J. Fluid Mech.* **205**, 341–358.

VAN ATTA, C. 1991 Local isotropy of the smallest scales of turbulent scalar and velocity fields. *Proc. R. Soc. Lond.* A **434**, 139–147.

VINCENT, A. & MENEGUZZI, M. 1991 The spatial and statistical properties of homogeneous turbulence. *J. Fluid Mech.* **225**, 1–20.

YAKHOT, V. 1994 Large-scale coherence and "anomalous scaling" of high-order moments of velocity differences in strong turbulence. *Phys. Rev.* E. **49**, 2887.

YAKHOT, V. & ORSZAG, S. A. 1986 Renormalization group analysis of turbulence. *J. Sci. Comput.* **1**, 3–51.

YAKHOT, V., ORSZAG, S. A., THANGAM, S., GATSKI, T. B. & SPEZIALE, S. G. 1992 Development of turbulence models for shear flows by a double expansion technique. *Phys. Fluids* A **4**, 1510–1520.